OPEN ACCESS
IOP Publishing
Reports on Progress in Physics
Rep. Prog. Phys. **87** (2024) 117801 (33pp)
https://doi.org/10.1088/1361-6633/ad7e4d

Observation of quantum entanglement in top quark pair production in proton–proton collisions at $\sqrt{s} = 13$ TeV

The CMS Collaboration

CERN, Geneva, Switzerland

E-mail: cms-publication-committee-chair@cern.ch

Received 6 June 2024, revised 18 September 2024
Accepted for publication 23 September 2024
Published 23 October 2024

Corresponding editor: Dr Lorna Brigham

Abstract

Entanglement is an intrinsic property of quantum mechanics and is predicted to be exhibited in the particles produced at the Large Hadron Collider. A measurement of the extent of entanglement in top quark-antiquark ($\mathrm{t\bar{t}}$) events produced in proton–proton collisions at a center-of-mass energy of 13 TeV is performed with the data recorded by the CMS experiment at the CERN LHC in 2016, and corresponding to an integrated luminosity of 36.3 fb^{-1}. The events are selected based on the presence of two leptons with opposite charges and high transverse momentum. An entanglement-sensitive observable D is derived from the top quark spin-dependent parts of the $\mathrm{t\bar{t}}$ production density matrix and measured in the region of the $\mathrm{t\bar{t}}$ production threshold. Values of $D < -1/3$ are evidence of entanglement and D is observed (expected) to be $-0.480^{+0.026}_{-0.029}$ ($-0.467^{+0.026}_{-0.029}$) at the parton level. With an observed significance of 5.1 standard deviations with respect to the non-entangled hypothesis, this provides observation of quantum mechanical entanglement within $\mathrm{t\bar{t}}$ pairs in this phase space. This measurement provides a new probe of quantum mechanics at the highest energies ever produced.

Keywords: CMS, top quark, entanglement

1. Introduction

Entanglement is a fundamental concept in quantum mechanics that describes a strong correlation between particles, such that the state of one particle cannot be independently described without considering the state of the other, regardless of the distance between them [1–3]. Quantum entanglement has been extensively studied in the context of photons and electrons [4–6]. In these measurements, entanglement is often determined through observations of particle properties, such as spin or polarization [7]. When considering the entanglement of two spin-1/2 particles, it is convenient to describe the quantum state of each particle as a linear combination of its basis states, usually denoted as $|0\rangle$ and $|1\rangle$ (corresponding to spin-up and spin-down states). In this formalism, one typically refers to each particle as a quantum bit (qubit) of information. An entangled state for two qubits is a superposition of their joint states that cannot be factorized into individual states. A common example is the Bell state, $|\psi^-\rangle = (|01\rangle - |10\rangle)/\sqrt{2}$, which can be realized to show the violation of Bell's inequality [8–10]. This state provides important insights into the Einstein–Podolsky–Rosen paradox [11], contributing to the ongoing discussion about the foundations of quantum mechanics. In a maximally entangled state, measuring the state of one qubit instantaneously determines the state

of the other, independent of the physical separation between them. The theoretical exploration of entanglement has recently been extended to collider settings involving a variety of fundamental particles including quarks, vector bosons, and the Higgs boson [12–23], as well as previously between taus produced from Z boson decays [24]. Observation of quantum entanglement and violation of Bell's inequality has also been established in neutral B meson decays [25].

Recently, the ATLAS Collaboration reported the first observation of entanglement in the top quark-antiquark ($\mathrm{t\bar{t}}$) system [26], with a result indicating a slight deviation from the standard model (SM) expectation. We focus on a measurement of entanglement in top quark pairs, which provides a new probe to test predictions of quantum mechanics at the highest energies currently accessible [27–29]. This result differs from the result reported by the ATLAS Collaboration in that we measure the entanglement at the parton level while the ATLAS Collaboration reports their observable at the particle level. Furthermore, the result presented here considers non-relativistic bound-state effects in the production threshold for the first time. The formation of such bound states can be linked to the Sommerfeld enhancement [30], which describes the increase in annihilation cross section due to the non-relativistic attractive potential between particles. In the context of $\mathrm{t\bar{t}}$ production, the Sommerfeld enhancement arises from the resummation of ladder diagrams involving gluon exchanges, which is partially accounted for in next-to-leading order (NLO) corrections. However, NLO corrections also include diagrams besides ladder diagrams such as the emission of real particles. The CMS result rests on performing a binned likelihood fit to extract the entanglement proxy instead of utilizing a calibration curve.

The SM of particle physics is expected to break down at extremely short distances since gravity needs to be reconciled with quantum mechanics at the Planck scale. Such a short distance is beyond the reach of particle colliders, but this result sheds light on quantum correlations at distances corresponding to energies of hundreds of GeV. Furthermore, measurements involving intrinsic spin are a powerful probe of beyond the SM (BSM) contributions to the production of $\mathrm{t\bar{t}}$ pairs in proton–proton (pp) collisions [31–37] and, possibly, at future circular lepton colliders [38]. Many of these BSM models alter the spin information of $\mathrm{t\bar{t}}$ pairs in complex and sizeable ways and, e.g. it has been shown in [33] that extensions of the SM implemented as an effective field theory can lower the level of entanglement of $\mathrm{t\bar{t}}$ pairs by up to 40% relative to the SM expectation. In contrast, BSM effects can contribute up to a 15% difference in the level of spin correlations of $\mathrm{t\bar{t}}$ pairs in the region $m(\mathrm{t\bar{t}}) > 600$ GeV, compared to the SM value in the same region. Hence, measurements of entanglement also provide a sensitive new probe of BSM contributions and represent a step towards quantum tomography and coherence measurements in top quark events [33].

In this article, a measurement of the entanglement of $\mathrm{t\bar{t}}$ events produced in pp collisions recorded with the CMS detector at a center-of-mass (CM) energy of 13 TeV at the CERN LHC is presented. The top quark is the heaviest known fundamental particle and has a very short lifetime. Expressed in natural units, the top quark's decay width $\Gamma_\mathrm{t} = 1.42^{+0.19}_{-0.15}$ GeV [39] is larger than the quantum chromodynamics (QCD) hadronization scale ($\Lambda_\mathrm{QCD} \sim 250$ MeV) and much larger than the spin decorrelation scale ($\Lambda^2_\mathrm{QCD}/m_\mathrm{t} \sim 0.36$ MeV, where m_t is the mass of the top quark) [40]. With such a large difference between the time scales of the top quark decay, the hadronization, and the spin decorrelation, the top quark spin retains its value from the moment it was created via the strong interaction. Thus, top quarks provide unique direct access to their spin information, which is carried by the angular distributions of their decay products. These angular distributions provide a probe of the entanglement of top quarks and the measurement presented here utilizes the same data set and treatment of systematic uncertainties as in [41], but with an optimized extraction technique to determine the extent of entanglement of top quarks and improved description of the production threshold region.

This article is structured as follows: section 2 covers the production and decay of top quarks, focusing on the $\mathrm{t\bar{t}}$ production threshold region. Section 3 explains the concept and significance of entanglement in top quark pairs, details the observable used to measure entanglement, and discusses the rationale for selecting the phase space region for this measurement. Section 4 outlines the CMS detector and provides details on identification and reconstruction of particles, while sections 5 and 6 provide information on the samples, analysis, and the background estimation. Section 7 discusses the systematic uncertainties, and section 8 introduces the pioneering modeling of the non-perturbative component of the $\mathrm{t\bar{t}}$ production threshold used in this analysis. Section 9 explains the technique for statistically determining whether $\mathrm{t\bar{t}}$ pairs are entangled. Results of the measurement are discussed in section 10, and a summary is given in section 11.

2. The production and decay of top quarks

At the LHC, top quarks are produced predominantly in pairs ($\mathrm{t\bar{t}}$) via the gluon-gluon (gg) fusion process and at a level of about 10% by quark-antiquark ($\mathrm{q\bar{q}}$) annihilation, both mediated by the strong interaction, as described with perturbative QCD calculations [42–45]. Figure 1 shows the representative leading order (LO) Feynman diagrams for $\mathrm{t\bar{t}}$ production via the strong force.

Top quarks are mostly unpolarized when produced via the strong force, but their spins are strongly correlated. The configuration of the top quark-antiquark spin is dependent on the invariant mass of the $\mathrm{t\bar{t}}$ pair ($m(\mathrm{t\bar{t}})$). The alignment (misalignment) of the spins of a top quark and a top antiquark results in like (unlike) helicity pairs, which dominate the low (high) invariant mass region. Top quark pairs originating from gg fusion at the production threshold correspond to the Bell state, i.e. they are maximally entangled spin-singlets, while $\mathrm{q\bar{q}}$

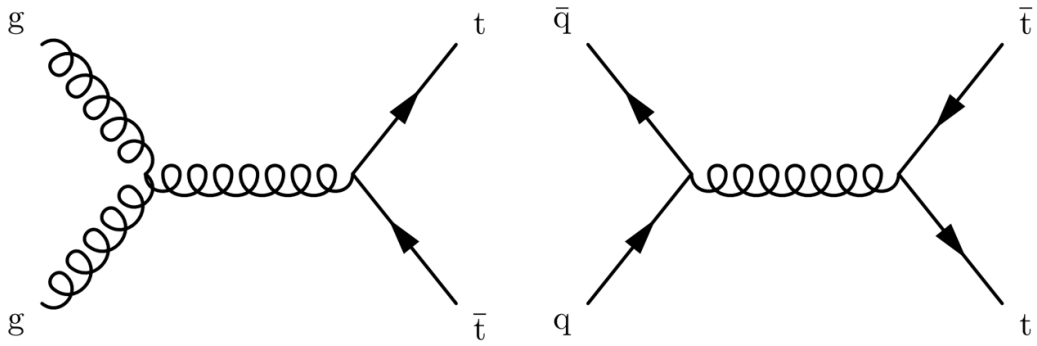

Figure 1. Representative leading order QCD Feynman diagrams for the $\mathrm{t\bar{t}}$ production through gg fusion (left) and quark-antiquark annihilation (right).

annihilation produces $\mathrm{t\bar{t}}$ pairs that are separable at the production threshold [27]. Thus, in the production threshold region $\mathrm{t\bar{t}}$ is produced in a mixed spin state. For a pure state, entanglement is a binary condition in which the pure state is non-separable. In contrast, for a mixed state, the degree of entanglement takes on a continuous value, measured via an entanglement witness or proxy, depending on the statistical ensemble of the individual states composing the mixed state. In this article, we exploit the $\mathrm{t\bar{t}}$ production threshold or 'low mass' region to carry out a measurement of the entanglement of top quarks using an entanglement proxy.

Just below the $\mathrm{t\bar{t}}$ production threshold of $2m_{\mathrm{t}} \approx 345\,\mathrm{GeV}$, where sensitivity to $\mathrm{t\bar{t}}$ entanglement is enhanced, QCD allows the formation of a so-far-unobserved bound state of a top quark and top antiquark, referred to as 'toponium' [46]. Such states are a prediction of the SM following from the experimentally confirmed existence of charmonium and bottomonium bound states [39]. Toponium bound states have yet to be discovered and they are not included in NLO QCD Monte Carlo (MC) simulations as toponium is inherently a non-perturbative phenomenon. An observed toponium resonance would be the sum of the ground state, η_{t}, and all other bound states, which are formed via nonrelativistic exchanges of gluons [47] that generate a Coulomb-like interaction between the top quarks. Including toponium in $\mathrm{t\bar{t}}$ production simulations is important in light of the recent ATLAS and CMS differential cross section results [48–52], which indicate difficulties in modeling the data near the $\mathrm{t\bar{t}}$ production threshold. The inclusion is also critical to this analysis as the pseudoscalar nature of toponium would lead to maximally entangled decay products.

Toponium production represents a distinct stage in the interaction dynamics between a top quark and antiquark, with both resonant color-singlet and nonresonant color-octet contributions. The total cross section—summed over all resonant and nonresonant contributions—is expected to peak at $m(\mathrm{t\bar{t}}) = 400\,\mathrm{GeV}$ and to fall off until around 700 GeV [53]. The color-singlet contribution is entirely dominated by the gg initial state and is predicted to form a pseudoscalar resonance, the resonant η_{t} state [54]. In the $\mathrm{t\bar{t}}$ production threshold region, the η_{t} state is predicted to form with a mass of 343 GeV and a production cross section of $6.43 \pm 0.90\,\mathrm{pb}$ [46, 55]. The width of the predicted η_{t} state, $\Gamma_{\eta_{\mathrm{t}}} = 7\,\mathrm{GeV}$, is determined from the difference between the QCD predictions with and without Coulombic corrections [46]. The η_{t} color-singlet contribution is not negligible when compared to the $\mathrm{t\bar{t}}$ cross section near the production threshold [37]. This is accounted for in this measurement by including a detailed study on the effect of the η_{t} state on the measurement of the entanglement present in $\mathrm{t\bar{t}}$ events.

In addition to this color-singlet resonant contribution, there are also color-octet contributions to toponium production [53], which become more significant at longer distances. These are dominated by gg initiated nonresonant color-octet pseudoscalar contributions and, to a smaller extent, $\mathrm{q\bar{q}}$-initiated resonant color-octet vector contributions. However, the color-octet contribution is subject to a repulsive potential and only forms a bound state after an additional gluon is either absorbed or emitted [56]. The latter complicates theoretical calculations of the octet contribution since these gluons are 'soft' and translate to a large value of the strong coupling constant (α_{S}). Hence, there is no comprehensive theory for toponium production and thus no MC simulation of the full bound-state spectrum. Owing to the lack of a model implementing these color-octet contributions, they are not included in the toponium model utilized here, which also applies to any interference terms. The phase space of the measurement presented here is selected to suppress $\mathrm{q\bar{q}}$ initiated processes, hence reducing the vector color-octet contributions to toponium production. Based on the state-of-the-art knowledge of toponium [54, 57], we estimate a systematic uncertainty of the toponium contribution in this measurement, which is explained in more detail in section 7. Furthermore, the predicted η_{t} state is a spin-singlet and therefore is expected to produce maximally entangled decay products in the phase space relevant for this analysis.

Top quarks decay almost exclusively via the electroweak interaction into a W^{+} boson and a bottom quark. Similarly, top antiquarks decay to a W^{-} boson and a bottom antiquark. This analysis targets events with two leptonic W boson decays, referred to as the 'dilepton' ($\ell^{+}\ell^{-}$) decay channel, where ℓ refers to electrons or muons, including those originating from the decay of τ leptons. Entanglement effects are probed through a spin-correlation analysis of the lepton pair.

The squared matrix element (ME) for $\mathrm{t\bar{t}}$ production and decay (with appropriate color and spin summation understood) [40, 58, 59] can be written as

$$|\mathcal{M}\left(\mathrm{q\bar{q}/gg} \to \mathrm{t\bar{t}} \to \left(\ell^+\nu\mathrm{b}\right)\left(\ell^-\bar{\nu}\bar{\mathrm{b}}\right)\right)|^2 \approx \mathrm{tr}\left[PR\overline{P}\right]. \quad (1)$$

In equation (1), tr is the trace, R is the production spin density matrix related to on-shell $\mathrm{t\bar{t}}$ production, and P and $\overline{P}$ are the decay spin density matrices for the top quark and top antiquark, respectively [58]. The narrow intrinsic width of the top quark allows the factorization of production and decay terms. According to [27], the most general form for the spin density operator ρ is given by:

$$\rho = \frac{1}{4}\left(I_4 + \sum_i \left(B_i^+\sigma^i \otimes I_2 + B_i^- I_2 \otimes \sigma^i\right) + \sum_{i,j} C_{ij}\sigma^i \otimes \sigma^j\right), \quad (2)$$

where I_n is the $n\times n$ identity matrix, σ^i refers to the Pauli matrices corresponding to each particle, and the indices i and j correspond to the three quantization axes ($i,j = 1,2,3$). The spin density operator ρ is related to R as $\rho = R/\mathrm{tr}(R)$. In the case of two spin-1/2 particles, in particular, in $\mathrm{t\bar{t}}$ production in pp collisions, $\mathbf{B}^{\pm}$ are 3-vectors that characterize the degree of top quark/antiquark polarization along each of the axes, and C is a 3×3 matrix that characterizes the correlation between the t and $\bar{\mathrm{t}}$ spins along each pair of axes. Given the on average net-zero polarization of $\mathrm{t\bar{t}}$ pairs near the $\mathrm{t\bar{t}}$ production threshold, the $\mathbf{B}^{\pm}$ vectors are not expected to be sensitive to entanglement in $\mathrm{t\bar{t}}$ production.

Working in the $\mathrm{t\bar{t}}$ CM frame, we use the helicity axis $\hat{k}$ defined by the top quark direction and the direction $\hat{p}$ of the incoming parton to define the direction perpendicular to the scattering plane $\hat{n} = (\hat{p}\times\hat{k})/\sin\Theta$, where Θ is the top quark scattering angle. The direction in the scattering plane mutually perpendicular to $\hat{k}$ and the transverse axis $\hat{n}$ is given by $\hat{r} = (\hat{p} - \hat{k}\cos\Theta)/\sin\Theta$. Although more details can be found in [41], for this article the relevant quantities for understanding the measurement are the scattering angle defined above and the opening angle between the charged decay leptons in their parent top quark rest frames, φ, which is independent of the coordinate system defined here.

Equation (1) can be translated into spin correlation observables in the coordinate system defined above. The cosine of the angle between the two charged decay leptons in their respective parent top quark rest frames, $\cos\varphi = \hat{\ell}^+\cdot\hat{\ell}^-$, has a linear relationship with the relative differential cross section

$$\frac{1}{\sigma}\frac{\mathrm{d}\sigma}{\mathrm{d}\cos\varphi} = \frac{1}{2}\left(1 - D\cos\varphi\right), \quad (3)$$

where the slope parameter D is the entanglement proxy considered in this analysis, which is described in section 3, and the spin analyzing power of the leptons is assumed to be unity [60].

3. Entanglement observable for top quark pairs

In general, measurements of top quark properties (specifically angular correlations) have been a highly sensitive probe as to whether the experimentally observed top quark is indeed the SM top quark [61]. Some top quark properties can be expressed as differential cross sections, for example distributions of spin correlation variables and hence the spin of top quarks is accessible via such distributions. In the realm of quantum measurements, it is possible to quantify varying degrees of entanglement within systems, influenced by factors such as phase space configurations and potential BSM contributions. This variability allows for a nuanced exploration of the hierarchy of quantum correlations within the spin density matrix, which can be conceptually organized as: Bell's inequality violation $\subseteq$ Entanglement $\subseteq$ Spin correlations. Compared to standard differential cross section measurements, estimating the systematic uncertainties relevant to conditions of entanglement requires—as it will be explained later—studies of different sources of systematic uncertainty and this can have quite a different impact on the measurement.

A quantum state of two subsystems, denoted α for the t quark and β for the $\bar{\mathrm{t}}$ antiquark, is separable when ρ can be expressed as a convex sum of tensor products of states between the respective subsystems, denoted as ρ_i^{α} and ρ_i^{β}. A necessary and sufficient condition for identifying entanglement in such a two-particle system is the Peres–Horodecki criterion [62, 63], which allows the identification of entanglement in systems composed of two particles by examining the partial transpose of ρ, given by $\rho^{\mathrm{T}_2} = \sum_i p_i\rho_i^{\alpha}\otimes(\rho_i^{\beta})^{\mathrm{T}}$, where p_i are the probabilities of the individual density operators. If ρ^{T_2} has any negative eigenvalues, then the state ρ is entangled. This criterion can be used to show that top quarks are entangled by measuring a proxy that takes on particular values when this criterion is met.

We consider the momenta of the two leptons in the CM frame of the $\mathrm{t\bar{t}}$ system and an additional boost into the frame of their respective parent top quark or antiquark. The momentum directions of the two leptons in these CM frames are labeled as $\hat{\ell}^+$ and $\hat{\ell}^-$. The four-fold angular distribution for the two charged leptons $\hat{\ell}^{+/-}$ in the t and $\bar{\mathrm{t}}$ reference frames is given by [64]

$$\frac{1}{\sigma}\frac{\mathrm{d}^4\sigma}{\mathrm{d}\Omega_+\mathrm{d}\Omega_-} = \frac{1}{(4\pi)^2}\left(1 + \mathbf{B}^+\cdot\hat{\ell}^+ + \mathbf{B}^-\cdot\hat{\ell}^- + \hat{\ell}^+\cdot\left(C\hat{\ell}^-\right)\right). \quad (4)$$

The charged lepton direction is used as a proxy for the top quark spin and the lepton is suitable for this purpose, since it has a spin analyzing power of $\approx$1 [60], which means that there is a strong correlation between the parent quark spin and the angular distribution of the lepton. For simplicity, the spin analyzing power factors are omitted in equation (4).

Both the polarization vectors $\mathbf{B}^{\pm}$ and the spin correlation matrix C depend on the specifics of the $\mathrm{t\bar{t}}$ kinematic variables. However, in this measurement we do not utilize the polarization vectors $\mathbf{B}^{\pm}$, since there is no net polarization of top quarks at LO and thus they are not expected to be sensitive

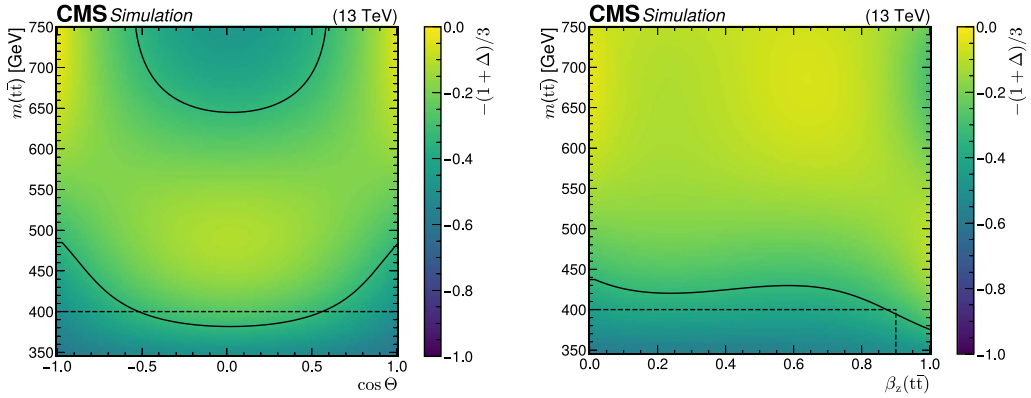

Figure 2. Predicted values of $-(1+\Delta)/3$ obtained from $\mathrm{t\bar{t}}$ MC simulation, without accounting for detector effects, are shown on the left as a function of $m(\mathrm{t\bar{t}})$ and the cosine of the top quark scattering angle Θ. The value of $-(1+\Delta)/3$ also determined by a $\mathrm{t\bar{t}}$ MC simulation as a function of $m(\mathrm{t\bar{t}})$ and $\beta_z(\mathrm{t\bar{t}})$ is shown on the right. In both figures the black solid lines represent the boundary for entanglement, while the black dashed line indicates the selected phase space in this analysis. The minimum value on the color axis of -1 corresponds to the boundary $\mathrm{tr}[C]=3$, a maximally entangled state. Top quarks with no spin correlations correspond to a value of $D=0$ and $\Delta=-1$ ($C=\mathbf{0}$). In the central boosted region, $D<-1/3$ is not a valid entanglement criterion as the negativity of the C_{11} and C_{22} elements is not guaranteed [66] and the correct entanglement criterion is $\Delta>0$.

to the entanglement of $\mathrm{t\bar{t}}$ pairs. Instead, we focus on the diagonal elements of the C matrix. At the production threshold, $\mathrm{t\bar{t}}$ production via gg fusion results in spin-singlet states, which means the quark spins are maximally correlated along any axis and C is diagonal: $C=\mathrm{Diag}(-1,-1,-1)$. Above threshold, the relative contribution of gg fusion resulting in spin-singlets decreases with increasing $m(\mathrm{t\bar{t}})$, resulting in more mixed states and diagonal elements of C that are less than one [65].

The Peres–Horodecki criterion relates an entanglement witness $\Delta\equiv -C_{33}+|C_{11}+C_{22}|-1$ to a condition for entanglement [27] of $\Delta>0$, where the third axis is taken as the spin quantization axis. The specific choice of which basis vector corresponds to the spin quantization axis can be chosen at will and ultimately results in four unique observables that can be used for entanglement measurements [37, 66].

The entanglement proxy, or D coefficient, is related to the diagonal C coefficients as:

$$D=\mathrm{tr}\,[C]/3=(C_{11}+C_{22}+C_{33})/3, \tag{5}$$

which yields the condition for observing entanglement:

$$\Delta+1=\mathrm{tr}\,[C]=-3D>1. \tag{6}$$

The coefficient D itself is a measure of the fraction of events where the spins of the t quark and $\bar{\mathrm{t}}$ antiquark are aligned. To demonstrate entanglement in top quark events, we compare the measured entanglement proxy D with the $-1/3$ boundary for entanglement in equation (6) [27]. Measuring $D<-1/3$ implies that the partial transpose of the density operator is not positive definite and therefore is nonseparable, which is following the criteria discussed in [63].

Figure 2 (left) illustrates how the entanglement is expected to vary as a function of the kinematic parameters. The quantity $-(1+\Delta)/3$ is shown (on the color scale) as a function of $m(\mathrm{t\bar{t}})$ and the top quark scattering angle Θ determined using a $\mathrm{t\bar{t}}$ MC simulation implementing both the gg fusion and $\mathrm{q\bar{q}}$ process at NLO. Intuitively, this means that at threshold, top quarks are produced in like-helicity states forming a spin-singlet state. This spin-singlet is maximally entangled and explains the large value of entanglement near the production threshold. Toward intermediate values of $m(\mathrm{t\bar{t}})$, the level of entanglement is substantially reduced, while at very high $m(\mathrm{t\bar{t}})$ the unlike-helicity states dominate and form a spin triplet state, which is also maximally entangled. We focus on the low $m(\mathrm{t\bar{t}})$ region, with $345<m(\mathrm{t\bar{t}})<400\,\mathrm{GeV}$, where we expect both C_{11} and C_{22} to be negative [59]. This simplifies the $\Delta>0$ entanglement criterion to $\mathrm{tr}[C]>1$.

It was suggested in [66] to enhance the purity of the gg fusion process by an additional requirement on the relative longitudinal velocity between the lab and $\mathrm{t\bar{t}}$ reference frames: $\beta_z(\mathrm{t\bar{t}})=|(p_z^{\mathrm{t}}+p_z^{\bar{\mathrm{t}}})/(E^{\mathrm{t}}+E^{\bar{\mathrm{t}}})|$. Figure 2 (right) shows again the quantity $-(1+\Delta)/3$ (on the color axis) as a function of $m(\mathrm{t\bar{t}})$ and $\beta_z(\mathrm{t\bar{t}})$. Below the dashed line indicates an entanglement sensitive phase space of $m(\mathrm{t\bar{t}})<400\,\mathrm{GeV}$ and $\beta_z(\mathrm{t\bar{t}})<0.9$.

For the measurement of entanglement in top quark events, we focus on a variable that can be measured more precisely [41], i.e. $\cos\varphi=\hat{\ell}^{+}\cdot\hat{\ell}^{-}$, which fully encapsulates the differential spin correlation information at the production threshold through the gg fusion process and in absence of BSM contributions [33].

At the $\mathrm{t\bar{t}}$ production threshold, the $\cos\varphi$ distribution provides the best sensitivity of all spin correlation variables and hence, the corresponding D coefficient is least affected by systematic uncertainties [41, 67]. The analysis strategy for measuring the entanglement in $\mathrm{t\bar{t}}$ pairs is based on using templates as a function of $\cos\varphi$ to perform a binned profile likelihood fit with uncertainties as nuisance parameters using the CMS statistical analysis tool COMBINE [68], which is based on the RooFit [69] and RooStats [70] frameworks. The final measured result in data is corrected to the

parton level and compared to the boundary for entangled top quark-antiquark states, which is well defined as $D = -1/3$. Therefore, observation of top quark entanglement at the parton level is equivalent to a measurement of D to be less than $-1/3$ within a given precision.

4. The CMS detector and event reconstruction

The central feature of the CMS apparatus is a superconducting solenoid of 6 m internal diameter, providing a magnetic field of 3.8 T. Within the solenoid volume are a silicon pixel and strip tracker, a lead tungstate crystal electromagnetic calorimeter (ECAL), and a brass and scintillator hadron calorimeter (HCAL), each composed of a barrel and two endcap sections. Forward calorimeters extend the pseudorapidity (η) coverage provided by the barrel and endcap detectors. Muons are measured in gas-ionization detectors embedded in the steel flux-return yoke outside the solenoid, with detection planes made using three technologies: drift tubes, cathode strip chambers, and resistive plate chambers. Events of interest are selected using a two-tiered trigger system [71]. The first level, composed of custom hardware processors, uses information from the calorimeters and muon detectors to select events at a rate of around 100 kHz within a time interval of less than 4 μs. The second level, known as the high-level trigger, consists of a farm of processors running a version of the full event reconstruction software optimized for fast processing, and reduces the event rate to around 1 kHz before data storage. A more detailed description of the CMS detector, together with a definition of the coordinate system used and the relevant kinematic variables, can be found in [72, 73].

A particle-flow (PF) algorithm [74] aims to reconstruct and identify each individual particle in an event, with an optimized combination of information from the various elements of the CMS detector. The primary vertex is taken to be the vertex corresponding to the hardest scattering in the event. The energy of photons is obtained from the ECAL measurement. The energy of electrons is determined from a combination of the electron momentum at the primary interaction vertex as determined by the tracker, the energy of the corresponding ECAL cluster, and the energy sum of all bremsstrahlung photons spatially compatible with originating from the electron track. The energy of muons is obtained from the curvature of the corresponding track. The energy of charged hadrons is determined from a combination of their momentum measured in the tracker and the matching ECAL and HCAL energy deposits, corrected for the response function of the calorimeters to hadronic showers. Finally, the energy of neutral hadrons is obtained from the corresponding corrected ECAL and HCAL energies.

Jets are reconstructed by clustering the PF candidates using the infrared- and collinear-safe anti-k_{T} clustering algorithm with a distance parameter of 0.4 [75, 76]. Jet momentum is determined as the vectorial sum of all particle momenta in the jet, and is found from simulation to be, on average, within 5%–10% of the true momentum over the whole transverse momentum (p_{T}) spectrum and detector acceptance. Additional pp interactions within the same or nearby bunch crossings (pileup) can contribute additional tracks and calorimetric energy depositions, increasing the apparent jet momentum. To mitigate this effect, tracks identified to be originating from pileup vertices are discarded and an offset correction is applied to correct for remaining contributions [77]. Jet energy corrections are derived from simulation studies so that the average measured energy of jets becomes identical to that of particle level jets. *In situ* measurements of the momentum balance in dijet, photon+jet, Z+jet, and multijet events are used to determine any residual differences between the jet energy scale (JES) in data and in simulation, and appropriate corrections are made [78]. Additional selection criteria are applied to each jet to remove jets potentially dominated by instrumental effects or reconstruction failures [77]. The jet energy resolution (JER) amounts typically to 15%–20% at 30 GeV and 10% at 100 GeV [78].

The missing transverse momentum vector $\vec{p}_{\mathrm{T}}^{\,\mathrm{miss}}$ is computed as the negative vector p_{T} sum of all the PF candidates in an event, and its magnitude is denoted as $p_{\mathrm{T}}^{\mathrm{miss}}$ [79]. The $\vec{p}_{\mathrm{T}}^{\,\mathrm{miss}}$ is modified to account for corrections to the energy scale of the reconstructed jets in the event.

Electron candidates, reconstructed from a combination of the track momentum vector at the primary interaction vertex and the corresponding clusters in the ECAL, are excluded if the ECAL clusters are in the region between the barrel and endcap ($1.44 < |\eta_{\mathrm{cluster}}| < 1.57$), since they have a reduced reconstruction efficiency there. A relative isolation criterion $I_{\mathrm{rel}} < 0.0588$ (0.0571) is applied for electron candidates in the barrel (endcap). The I_{rel} is defined as the p_{T} sum of all photon and neutral and charged hadron candidates within a distance of 0.3 from the electron candidate in η-φ space, divided by the p_{T} of the electron candidate, with a correction to suppress the residual effect of pileup. Additional electron identification requirements are applied to reject misidentified electron candidates and candidates originating from photon conversions [74, 80]. The electron momentum is estimated by combining the energy measurement in the ECAL with the momentum measurement in the tracker. The momentum resolution for electrons with $p_{\mathrm{T}} \approx 45$ GeV from $\mathrm{Z} \to \mathrm{ee}$ decays ranges from 1.6%–5%. It is generally better in the barrel region than in the endcaps, and also depends on the bremsstrahlung energy emitted by the electron as it traverses the material in front of the ECAL [81, 82].

Muon candidates are reconstructed using the track information from the tracker and the muon system [83]. A relative isolation requirement of $I_{\mathrm{rel}} < 0.15$ within a distance of 0.4 in η-φ space from the muon candidate is applied. To reject misidentified muon candidates and candidates originating from decay-in-flight processes, additional muon identification requirements are used [83]. The efficiency to reconstruct and identify muons is greater than 96%. Matching muons to tracks measured in the silicon tracker results in a relative p_{T} resolution of 1 (3)% in the barrel (endcaps) for muons with p_{T} up to 100 GeV.

5. Data and simulated samples

The analysis is performed using 36.3 fb^{-1} of pp collision data collected by the CMS experiment during the 2016 LHC run at a CM energy of 13 TeV. The single muon trigger efficiency exceeds 90% over the full η range. To maximize the trigger efficiency, both single-lepton and dilepton triggers are used. Data events are required to pass one of the following dilepton or single lepton triggers. For events containing two reconstructed electrons with opposite charge, the p_{T} of the leading (sub-leading) electron is required to be larger than 23 (12) GeV. For events containing two reconstructed oppositely charged muons, the p_{T} of the leading (sub-leading) muon is required to be larger than 17 (8) GeV. For events containing a reconstructed electron and a muon, either the muon p_{T} is required to be greater than 23 GeV and the electron p_{T} greater than 12 GeV or the muon p_{T} is required to be greater than 8 GeV and the electron p_{T} greater than 23 GeV. The dilepton triggers additionally require the reconstructed z coordinate of the vertex position of the leptons to be within 0.2 cm of each other. The single lepton triggers require the electron p_{T} to be greater than 27 GeV and the muon p_{T} greater than 24 GeV.

We utilize a combined simulated signal sample consisting of a (dominant) $\text{t}\bar{\text{t}}$ contribution and the η_{t} contribution, for the top quark bound state described in section 2. The $\text{t}\bar{\text{t}}$ signal sample is produced using the POWHEGV2 event generator at NLO [84–87] including spin correlations and thus referred to as the 'spin correlated' (SC) or 'nominal $\text{t}\bar{\text{t}}$' sample. The nominal $\text{t}\bar{\text{t}}$ sample is reweighted to a POWHEGV2 sample with spin correlations turned off differentially in $m(\text{t}\bar{\text{t}}) \otimes \cos\varphi \otimes \beta_z(\text{t}\bar{\text{t}}) \otimes \cos\Theta$, with otherwise the exact same settings, to implement the $\text{t}\bar{\text{t}}$ 'no spin correlation' (noSC) case. We rely on the TOP++ v2.0 program [42] to calculate the $\text{t}\bar{\text{t}}$ production cross section at next-to-NLO (NNLO) including electroweak (EWK) corrections at NLO, and obtain $832^{+20}_{-29}\,(\text{scale}) \pm 35\,(\text{PDF}+\alpha_{\text{S}})$ pb assuming $m_{\text{t}} = 172.5$ GeV. In order to assess the level of variation when using an alternative ME and matching procedure, a second $\text{t}\bar{\text{t}}$ sample is obtained using MADGRAPH5_aMC@NLO version 2.4.2 (MG5_aMC@NLO) [88] including MADSPIN [89] at NLO, where the ME jets are matched to parton showers using the FxFx prescription [90]. The parton distribution functions (PDFs) in all cases are described using NNPDF3.0 [91], and m_{t} is assumed to be 172.5 GeV.

The η_{t} signal sample is produced using the MADGRAPH5_aMC@NLO version 2.6.5 event generator at LO [46] including spin correlations. The η_{t} particle couples exclusively to gluons and top quarks and is produced through an s-channel process resulting in a $\text{t}\bar{\text{t}}$ pair. In the production threshold region, this calculation predicts the η_{t} to form with a mass of 343 GeV and width of 7 GeV with a production cross section of 6.43 pb [46]. This η_{t} signal sample is produced at parton level selecting only events with masses in between 337–349 GeV. The generator-level events in the simulated η_{t} sample are smeared to the reconstruction level utilizing the nominal $\text{t}\bar{\text{t}}$ sample. To get a noSC η_{t} sample, the nominal MADGRAPH5_aMC@NLO version 2.6.5 η_{t} sample is reweighted using the same procedure that was applied to the nominal POWHEGV2 $\text{t}\bar{\text{t}}$ sample.

The combined signal model of $\text{t}\bar{\text{t}}+\eta_{\text{t}}$ includes corrections to account for EWK contributions at NLO, referred to as 'EWK corrections', and the corrections to the average of the transverse momentum of the top quark and top antiquark ($p_{\text{T}}(\text{t}/\bar{\text{t}})$) spectra derived from NNLO QCD. For the $p_{\text{T}}(\text{t}/\bar{\text{t}})$ reweighting, also referred to as 'NNLO QCD reweighting', we use FASTNLO tables [92–94] to compute the $p_{\text{T}}(\text{t}/\bar{\text{t}})$ distribution in fixed-order QCD at NNLO using the same PDF and m_{t} value as was used in the $\text{t}\bar{\text{t}}$ sample but excluding EWK contributions at NLO, since those are applied in a separate additional step. The EWK corrections are taken into account by following a similar approach as in [95] to determine the size and uncertainty of these corrections (discussed in section 7). The EWK corrections are computed in HATHOR at NLO differentially in $\cos\Theta$ and $m(\text{t}\bar{\text{t}})$. The generator level values of $m(\text{t}\bar{\text{t}})$ and $\cos\Theta$ are used to determine the appropriate $\kappa^{\text{EWK}}_{\text{NLO}}$ scale factor (SF) per event. Applying these EWK corrections on a bin-by-bin basis can be performed via two different methods: 'multiplicative' or 'additive'. The multiplicative approach determines a SF, $\kappa^{\text{EWK}}_{\text{NLO}}$, that is applied multiplicatively to the nominal $\text{t}\bar{\text{t}}$ sample, while the additive approach adds the predicted EWK contribution to the nominal $\text{t}\bar{\text{t}}$ sample. In most regions of the kinematic phase space, the EWK contributions to the differential cross section factorize, and therefore the multiplicative approach is a good approximation to correct for higher-order EWK contributions. However, the difference between the two approaches is taken as a systematic uncertainty.

The major sources of background contributions are Z+jets, single top quark tW, dibosons (WW, WZ, and ZZ), and $\text{t}\bar{\text{t}}$ events in association with W/Z bosons ($\text{t}\bar{\text{t}}\text{V}$). The Z+jets sample is simulated at NLO with MG5_aMC@NLO (FxFx matching) [90], single top quark samples are produced at NLO with POWHEGV2, diboson events are simulated at LO with PYTHIA 8.219 [96], (referred to as PYTHIA8 in what follows), and $\text{t}\bar{\text{t}}\text{V}$ samples are produced at NLO with MG5_aMC@NLO (FxFx matching).

For all signal and background samples, the parton showering and hadronization is performed with PYTHIA8. While the PYTHIA8 CUETP8M2T4 tune [97] is employed to describe the underlying event in the $\text{t}\bar{\text{t}}$, η_{t}, and single top quark samples, all other background samples utilize the PYTHIA8 CUETP8M1 tune [98]. An alternative showering and hadronization model, HERWIG++ [99], is used to quantify the sensitivity to the modeling of these processes. Where HERWIG++ is used for parton showering and hadronization, the EE5C tune [100] is employed instead.

Pileup collisions are overlaid to each simulated event, and the generated distribution of the number of events per bunch crossing is matched to that observed in data. The full CMS detector simulation is carried out using GEANT4 version 9.4 [101].

6. Event selection, background estimation, and kinematic reconstruction

The measurement of the entanglement proxy D employs, to a large extent, the event selection and approaches to background estimation and corrections as in [41, 49], which measured D at the inclusive level to be 0.237 ± 0.011 [41], indicating no entanglement over the full phase space. For this measurement, the $\mathrm{t\bar{t}}$ pairs are restricted to a phase space where the level of entanglement is expected to be high and the selection is optimized to enhance entangled top quarks as discussed later in this section.

Both electron and muon candidates are required to have $p_\mathrm{T} > 25$ (20) GeV for the leading (trailing) candidate and $|\eta| < 2.4$. Electrons and muons originating from tau lepton decays are considered as signal for this analysis. Jets are selected if they have $p_\mathrm{T} > 30\,\mathrm{GeV}$ and $|\eta| < 2.4$ with additional isolation requirements.

Jets originating from the hadronization of b quarks (b jets) are identified (b tagged) by combining information related to secondary decay vertices reconstructed within the jets and track-based lifetime information in an algorithm (CSVv2) that provides the b jet identification efficiency of 79%–87% and a probability to misidentify light- and charm-flavor jets as b jets of approximately 10% and 40%, respectively [102].

The selected events are required to have exactly two isolated electrons or muons of opposite electric charge and at least two jets. At least one of the jets is required to be b tagged. Events with a lepton-pair invariant mass $m(\ell^+\ell^-) < 20\,\mathrm{GeV}$ are removed in order to suppress contributions from heavy-flavor resonance decays and low-mass Drell–Yan processes. In the $\mathrm{e^+e^-}$ and $\mu^+\mu^-$ channels, backgrounds from Z+jets processes are further suppressed by requiring $p_\mathrm{T}^\mathrm{miss} > 40\,\mathrm{GeV}$ and vetoing events in the Z boson mass region, with $76 < m(\ell^+\ell^-) < 106\,\mathrm{GeV}$. The remaining background yield from Z+jets events, which is large in the $\mathrm{e^+e^-}$ and $\mu^+\mu^-$ channels, is determined by applying a factor derived from simulation to the number of Z+jets events observed in data in a control region where $m(\ell^+\ell^-)$ is close to the Z boson mass [103]. A correction to account for non-Z+jets backgrounds in the control region is derived from the $\mathrm{e^\pm}\mu^\mp$ channel. The simulated Z+jets yield is corrected by a SF of up to 1.05 in each channel to match the determination from data.

Other background sources include processes of diboson, single top quark tW, and $\mathrm{t\bar{t}}$+Z/W ($\mathrm{t\bar{t}V}$) production, as well as misidentified $\mathrm{t\bar{t}}$ events originating from lepton+jets and hadronic decay channel events. These $\mathrm{t\bar{t}}$ events are collectively referred to as '$\mathrm{t\bar{t}}$ other'. The same category for the η_t only consists of 11 events. Hence, it is negligible compared to the η_t signal component of 892 events and not included.

The number of W+jets events is found to be negligible (<0.5%) and hence is not included as a background source. Overall, the event selection as described here has a purity of >88%.

To determine the most sensitive phase space for measuring the entanglement proxy D while minimizing expected total uncertainties, we scan the phase space of $\cos\varphi \otimes m(\mathrm{t\bar{t}}) \otimes \beta_z(\mathrm{t\bar{t}})$. The region with the highest expected sensitivity is determined based on maximizing the expected sensitivity to observe entangled $\mathrm{t\bar{t}}$ pairs. We converge on a best choice of $345 < m(\mathrm{t\bar{t}}) < 400\,\mathrm{GeV}$ along with an additional requirement of $\beta_z(\mathrm{t\bar{t}}) < 0.9$, shown in figure 2 with the dashed lines. The final event yields displayed in table 1 are obtained after applying all selection requirements.

Table 1. The expected number of events from signal and background contributions after event selection, compared with the number observed in data. The '$\mathrm{t\bar{t}}$ other' category includes mis-identified semileptonic and fully hadronic decays, and hadronic decays of tau leptons of the $\mathrm{t\bar{t}}$ pairs. The uncertainties include only the MC statistical uncertainties. The 'Only η_t' contribution is not added to the total MC prediction since it is included in the combined ($\mathrm{t\bar{t}}$+η_t) signal contribution.

Sample	Full phase space	$345 < m(\mathrm{t\bar{t}}) < 400\,\mathrm{GeV}$ & $\beta_z(\mathrm{t\bar{t}}) < 0.9$
Signal ($\mathrm{t\bar{t}}$+η_t)	$230\,580 \pm 210$	$45\,793 \pm 92$
Z+jets	$11\,300 \pm 400$	3560 ± 260
tW	8990 ± 110	1873 ± 49
$\mathrm{t\bar{t}}$ other	1916 ± 19	572 ± 10
Diboson	711 ± 19	179.6 ± 9.4
$\mathrm{t\bar{t}V}$	691.6 ± 5.8	100.1 ± 2.1
Total MC	$254\,190 \pm 500$	$52\,080 \pm 300$
Only η_t	1554.4 ± 6.9	892.2 ± 6.0
Data	255 646	53 843

All of the background contributions except those from Z+jets are estimated from simulation following [41].

The yields from simulation are normalized to the integrated luminosity of 36.3 $\mathrm{fb^{-1}}$. Data-to-simulation SFs are applied to simulated events to account for trigger, lepton, b tagging, and kinematic reconstruction efficiencies.

The four-momenta of the t and $\mathrm{\bar{t}}$ in each event are estimated using a kinematic reconstruction algorithm [49, 104]. The algorithm solves for the unknown neutrino momenta under these constraints: $p_\mathrm{T}^\mathrm{miss}$ is attributed solely to the two neutrinos; the invariant mass of each W boson, m_W, is fixed to 80.4 GeV [39]; and the invariant mass of each top quark must equal 172.5 GeV. Detector resolution effects are modeled by smearing the measured energies and directions of jets and leptons based on their simulated resolutions, and m_W is smeared according to a relativistic Breit–Wigner distribution with a width of 2.1 GeV [39]. The best-fit solution for neutrino momenta is selected based on the smallest reconstructed $m(\mathrm{t\bar{t}})$, and solutions are weighted by the expected invariant mass spectrum of the lepton and b jet system ($m(\ell\mathrm{b})$) from the top quark decay [49] after the kinematic selection requirements. Weights from 100 smearings are used to compute the four-momenta as a weighted average. This reconstruction is performed for all suitable pairs of b jet candidates for the two possible lepton-jet assignments. Only if no kinematic solution is found at all, then also combinations with one b-tagged and one untagged jet are considered. The jet pair and lepton-jet assignment that yields the maximum sum of weights is chosen. The kinematic reconstruction efficiency is about 90% in both data and simulation; the remaining 10% are events without a real neutrino momenta solution.

7. Systematic uncertainties

In this section, each of the uncertainties in the measurement of the top quark entanglement proxy D is discussed. For each source of systematic uncertainty, templates as a function of $\cos\varphi$ are generated based on ±1 standard deviation (σ) uncertainty variations and table 2 shows a summary of systematic uncertainties and their impact on the measurement at the pre-fit level. The templates are used as inputs for a binned profile likelihood fit.

7.1. Experimental uncertainties

In order to improve the description of the data by the simulation, efficiency SFs ($\mathrm{SF} = \epsilon_{\mathrm{DATA}}/\epsilon_{\mathrm{MC}}$) are applied where necessary. Most SFs are applied as event weights to the simulated samples.

Trigger efficiencies (for the OR of the dilepton and single-lepton triggers) are measured as a function of the lepton η using triggers that are only weakly correlated with the dilepton triggers ($p_{\mathrm{T}}^{\mathrm{miss}}$-based triggers). Measurements from data are used to improve predictions from Z+jets simulation. The measured SFs are typically close to unity across all bins. Uncertainties related to trigger efficiency SFs are measured using two kinds of variations, following the same procedure as in [49]. First, the SFs are varied according to their uncertainties in order to account for the change in total rates with respect to the nominal simulation. The second kind of variation accounts for the shape modification. This is achieved by varying the SFs with 'up' and 'down' variations, based on the different combinations of dilepton η regions. An envelope of the two variations is constructed to determine the uncertainty.

Lepton identification and isolation efficiencies (referred to as 'Lepton ident./isolation') for electrons and muons are estimated as a function of p_{T} and η using a 'tag-and-probe' method [105, 106] based on the Z boson samples. The SFs are found to be close to unity and they are varied according to their uncertainties.

Tagging efficiencies for b, c, and light-quark or gluon jets (referred to as 'b tagging (heavy)' and 'b tagging (light)', respectively) are determined from simulation as a function of jet p_{T} and η [102]. Since the b tagging efficiencies measured in data are different from those measured in simulation, SFs are applied to the simulated events. Envelopes of the normalization and shape uncertainties are calculated for both the heavy and light flavors and these are used independently as input templates to the profile likelihood fit.

For a fraction of events (about 9%), the $\mathrm{t\bar{t}}$ kinematic reconstruction finds no physical result as the only solutions to the quadratic equation are imaginary and the events are rejected. This occurs because of resolution effects and the top quark and W boson mass constraints. The efficiency is expressed as a function of lepton observables (p_{T} and η), the number of b jets, and $p_{\mathrm{T}}^{\mathrm{miss}}$. The data-to-simulation SFs are derived separately for the ee, $\mu\mu$, and eμ final states. Uncertainties are estimated following the procedure in [49].

The uncertainties due to the JES are determined from 19 JES sources [78]. These sources arise from differences due to variations of the energy of the reconstructed jets ('JES: Absolute' and 'JES: Absolute (stat)') and pileup offset dependence ('JES: pileup') in simulated events between different detector regions, as well as due to corrections for initial- (ISR) and final-state radiation (FSR), and also due to uncertainties in the correction factors of heavy- and light-flavor jets ('JES: Relative samples' and 'JES: Flavor QCD'). 'JES: Relative Balance' accounts for the difference in modeling of missing transverse momentum. Simulations are run with jet four-momenta scaled by the corresponding uncertainties to obtain 'up' and 'down' systematic samples. Variations of the jet four-momenta are propagated to $p_{\mathrm{T}}^{\mathrm{miss}}$ measurements. The selection efficiency is recalculated with rescaled simulated samples and the difference with respect to the original samples is taken as systematic uncertainty for the relevant JES source.

The JER is smeared using a scaling method whereby the difference between the reconstructed jet p_{T} and the matched generated jet p_{T} is scaled by a certain factor. Uncertainties in the correction factors are evaluated accordingly. The simulated JER is varied by $\pm1\sigma$ uncertainty in different η regions [78].

The energy deposited by charged and neutral hadrons and photons is varied according to their energy resolutions, and the $p_{\mathrm{T}}^{\mathrm{miss}}$ four-vectors are recalculated to account for the unclustered $p_{\mathrm{T}}^{\mathrm{miss}}$ (referred to as 'Unclustered energy').

The pileup effect on the signal efficiency is accounted for by varying the total inelastic cross section by $\pm4.6\%$ with respect to the nominal value of 69.2 mb [107].

The normalization of the background events represents another source of systematic uncertainty, estimated by using the corresponding experimental uncertainties per background source. This uncertainty is assigned a log-normal prior. In the ee and $\mu\mu$ channels, the background from Z+jets processes is dominant. Its normalization (referred to as 'Z+jets normalization') is varied by $\pm20\%$ [105]. A data-driven approach is applied to estimate this uncertainty where the MC prediction in the Z boson mass region is compared to data at different points during the selection, which yields a SF of up to 1.2 applied to the Z+jets sample, and the full size of that SF is taken as a 20% normalization uncertainty. In addition, a shape uncertainty (referred to as 'Z+jets shape') is determined to cover differences in modeling Z+jets production at LO and NLO. The NLO Z+jets sample is used to determine a slope in the $\cos\varphi$ distribution and a $\pm5\%$ variation is applied to derive up/down templates.

Finally, the uncertainty in the integrated luminosity for 2016 data (1.2%) [108] is propagated to the normalization of all simulated predictions including $\mathrm{t\bar{t}}$ and η_{t}.

7.2. Model uncertainties

The impact of theoretical assumptions on the modeling is determined by considering uncertainties that affect both the normalization and shape and those that affect only the normalization. The former are parametrized by nuisances with Gaussian priors and the latter by nuisances with log-normal priors.

Table 2. An overview of the systematic uncertainties and their impact on the yields and shape of the $\cos\varphi$ distribution. The uncertainties are categorized by their type where 'norm.' refers to normalization uncertainties modeled with a log-normal prior and 'shape' refers to shape uncertainties. The impact on the yields and shape of the $\cos\varphi$ distribution is given in percent where the difference in the shape of the $\cos\varphi$ distribution is determined from the forward-backward asymmetry. The JES systematics are split as in [78] with the addition of 'JES: Relative Balance' accounting for the difference in modeling of missing transverse momentum.

Uncertainty category	Type	Effect on yield	Effect on shape
Experimental uncertainties			
Trigger efficiency	Shape	0.5%	0.2%
Lepton ident./isolation	Shape	3.0%	0.2%
b tagging (heavy)	Shape	0.6%	0.1%
b tagging (light)	Shape	0.3%	0.2%
Kinematic reconstruction	Shape	0.3%	0.1%
JES: Absolute	Shape	0.9%	0.3%
JES: Absolute (stat)	Shape	0.4%	0.2%
JES: Pileup	Shape	0.5%	0.2%
JES: Flavor QCD	Shape	0.7%	0.2%
JES: Relative balance	Shape	0.4%	0.8%
JER	Shape	0.3%	0.3%
Unclustered energy	Shape	0.2%	0.3%
Pileup	Shape	0.4%	0.1%
$\mathrm{t\bar{t}}$ normalization	Norm.	4.4%	0.3%
Z+jets normalization	Norm.	1.6%	0.4%
Z+jets shape	Shape	0.2%	0.2%
Luminosity	Norm.	1.2%	<0.1%
Model uncertainties			
Matrix-elem. renorm. scale variation	Shape	0.4%	0.3%
Matrix-elem. fact. scale variation	Shape	0.6%	0.2%
Parton shower: Initial-state radiation	Shape	0.8%	0.7%
Parton shower: Final-state radiation	Shape	2.1%	0.4%
Top quark mass	Shape	2.4%	0.5%
ME/parton shower matching	Norm.	0.8%	<0.1%
Underlying event	Norm.	0.8%	<0.1%
PDF	Shape	0.9%	0.1%
Color reconnection	Norm.	0.8%	<0.1%
b quark fragmentation	Shape	0.7%	0.4%
B hadron semilept. decays	Shape	0.3%	0.2%
Branching fraction	Norm.	1.9%	<0.1%
NNLO QCD reweighting	Shape	0.6%	0.4%
EWK corrections	Shape	0.6%	0.4%
η_t normalization	Norm.	0.7%	0.8%
η_t binding energy	Shape	0.2%	0.1%

Renormalization and factorization scales in the ME calculation in POWHEGV2 samples (referred to as 'Matrix-elem. renorm. scale variation' and 'Matrix-elem. fact. scale variation', respectively) are varied considering the following variations as a function of the $\cos\varphi$ distribution:

- μ_R is fixed, μ_F is varied by 2.0 (0.5) for the up (down) shape;
- μ_F is fixed, μ_R is varied by 2.0 (0.5) for the up (down) shape.

To evaluate the impact of the choice of the α_S value in the parton shower (PS) simulation, dedicated POWHEGV2+PYTHIA8 samples are used.

The uncertainties associated with the modeling of ISR and FSR are estimated with the separate up/down variations of the $\alpha_\mathrm{S}^\mathrm{ISR}$ or $\alpha_\mathrm{S}^\mathrm{FSR}$ parameter in the dedicated samples, changing their scale individually up and down by factors of 2 and $\sqrt{2}$, respectively. For ISR and FSR uncertainties we use the up and down variations to determine a template representing a shape uncertainty from a linear fit to these variations. The slope parameters determined from these linear fits to the $\cos\varphi$ distribution are -0.0078 ± 0.0060 (ISR) and -0.0021 ± 0.0033 (FSR). From these slope parameters, we derive symmetrized templates representing a shape uncertainty due to ISR and FSR effects (referred to as 'Parton shower: Initial-state radiation' and 'Parton shower: Final-state radiation', respectively).

Two POWHEGV2 samples are used to estimate the impact of the value used for m_t in the MC sample on signal selection efficiency. Compared to the $\mathrm{t\bar{t}}$ POWHEGV2 sample, these two

have identical settings but different values of m_t and are used to derive templates corresponding to the down and up variations of m_t by 0.5 GeV.

Two MG5_aMC@NLO η_t samples are used to estimate the impact of m_t in the η_t process. Also, identical settings are used for these η_t samples except for m_t. These samples are used to derive templates corresponding to the down and up variations of m_t by 0.5 GeV.

To account for the uncertainty due to ME-PS matching (referred to as 'ME/parton shower matching'), the h_{damp} parameter is varied up and down by one σ with respect to its default value of $h_{damp} = 1.58^{+0.66}_{-0.59} m_t$ in the POWHEGV2+PYTHIA8 simulation [97]. As no significant shape effect is observed but the linear fit yields a normalization effect of typically <1%, we model this effect as a 1% uncertainty with a log-normal prior in the $t\bar{t}$ normalization.

The uncertainty due to the underlying event tune (referred to as 'Underlying event') is measured using the POWHEGV2+PYTHIA8 simulations with up/down variations of the tune parameters with respect to its default value according to their uncertainties [109]. Again, a linear fit of the $\cos\varphi$ distribution of these up/down variations is utilized to determine a shape uncertainty. A <1% flat effect is observed and hence, is assigned an uncertainty of 1% with a log-normal prior.

The uncertainty arising from the PDFs is assessed by reweighting the $t\bar{t}$ signal sample according to the 100 replicas in the NNPDF3.0 PDF set. Also, the α_S value used in the NNPDF3.0 PDF set is varied separately according to its uncertainties.

A multiple particle interaction (MPI) scheme with early resonance decays switched off is implemented in the PYTHIA8 simulation of the $t\bar{t}$ process as a default color reconnection model. Various color reconnection models (MPI-based scheme with early resonance switched on, gluon-move scheme, and QCD-inspired scheme) [110, 111] are applied to the signal sample independently. Since no significant shape effect is observed, a log-normal prior on the $t\bar{t}$ normalization of 1% is assigned as uncertainty for color reconnection.

The Bowler–Lund function [112, 113] with a parameter value of 0.855 [114] is used as a default fragmentation function to describe momentum transfer from b quarks to B hadrons in the $t\bar{t}$ simulation. The effect of an up and down variation of the Bowler–Lund function is studied by reweighting the relevant transfer function at the generator level of the $t\bar{t}$ sample. Furthermore, a different fragmentation function (Peterson function [39]) is used as an alternative function to reweight the signal sample. A shape dependent total uncertainty due to the fragmentation model (referred to as 'b quark fragmentation') is estimated by taking an envelope of the results from the two approaches.

The semileptonic branching fraction (BF) of B hadrons could affect the b jet energy response. The b jets with semileptonic B hadron decays (referred to as 'B hadron semilept. decays') are reweighted at the generator level by comparing the PYTHIA8 BFs with the ones taken from PDG 2022 [39] and their uncertainties. More details on these effects are provided in [115]. This effect results in a shape uncertainty.

The combined dileptonic BF for the $t\bar{t}$ decay into ee, $\mu\mu$, and eμ final states including leptonic decays of τ leptons is $\mathcal{B}_{combined} = 0.06425$ with an uncertainty (referred to as 'Branching fraction') of 1.8% [39], and this is assigned a log-normal prior.

We reweight the nominal signal MC sample such that the top quark p_T spectrum matches that from a fixed-order ME calculation at NNLO in QCD. The nominal signal MC sample without this NNLO QCD reweighting is taken as the systematic variation in the NNLO QCD reweighting. Since this is a one-sided variation, we supply this as the positive variation in the fit and restrict the fit to only consider the positive variation.

An uncertainty in the EWK corrections is included to account for contributions from higher mixed-order terms, following the same prescription as outlined in [95] and allowing us to estimate the impact of missing higher-order terms in the ME calculations. The EWK corrections are applied to the $t\bar{t}$ signal sample using the multiplicative approach and the uncertainty is taken as the difference between the multiplicative and additive approaches. Since this is a one-sided variation, we supply this as the positive variation in the fit and restrict the fit to only consider the positive variation.

We assign specific systematic uncertainties to compensate for the unknown η_t signal component with respect to its normalization and shape. The expected migration between bins of the $\cos\varphi$ distribution is obtained from simulated $t\bar{t}$ events at reconstruction level and used to smear the generator-level events in the simulated η_t sample.

In order to determine a model uncertainty for the toponium contribution we rely on a theoretical result in [54]. The normalized $m(t\bar{t})$ cross section distribution between 300 and 380 GeV, which is predicted at NLO plus next-to-leading power [57] (NLO+NLP) and NNLO+NLP levels, is compared with earlier results using CMS data [49] and shows reasonable agreement when applying a SF of 1.2. However, the toponium model at LO QCD utilized in this measurement only uses the η_t color-singlet contribution and does not adequately cover effects of color-octet contributions. Hence, we vary the η_t cross section by ±50% of its predicted value to account not just for resummation effects, but also for the effects described earlier. The predictions for the binding energy of η_t under various potentials has been shown to vary from −1.7 to −2.6 GeV [116]. Thus, we also vary the binding energy of the η_t by ±0.5 GeV, which directly influences the formation and stability of the $t\bar{t}$ bound state and quantifies the energy required to separate the top quark and antiquark constituents, impacting the shape of the η_t signal component. The choice of the size of this variation ensures that the model returns physical solutions with a negative binding energy in the variation. Missing color-octet contributions are also affected by variations of the binding energy, but this effect is included in the overall normalization uncertainty.

8. Modeling of the production threshold

Several kinematic variables, shown in figure 3, were examined to study the modeling of the data by the MC simulation

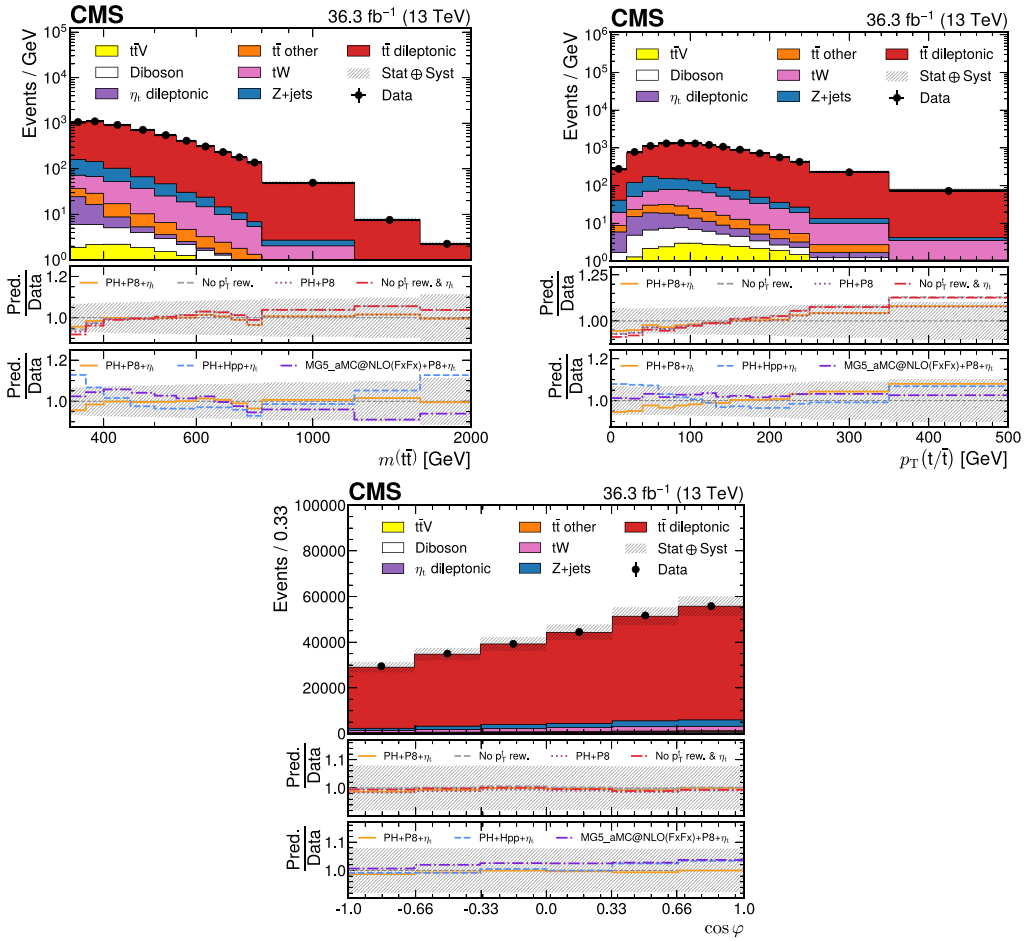

Figure 3. Reconstruction-level $m(\mathrm{t\bar{t}})$ (upper left), $p_\mathrm{T}(\mathrm{t}/\bar{\mathrm{t}})$ (upper right), and $\cos\varphi$ (lower) distributions of the combined signal model (POWHEGV2+PYTHIA8+η_t, labeled PH+P8+η_t) in the full phase space comparing the modeling of the data by MC simulation when not including η_t contributions (purple dotted line in the upper panel under each plot), or no $p_\mathrm{T}(\mathrm{t}/\bar{\mathrm{t}})$ reweighting is applied (gray dashed line in the upper panel), or neither of those (red dashed-dotted line in upper panel). The lower panel under each plot compares the data to POWHEGV2+HERWIG++ (blue dashed line, labeled PH+Hpp+η_t), to MG5_aMC@NLO (FxFx)+PYTHIA8 (purple dashed-dotted line), and finally to the nominal MC including η_t contributions and $p_\mathrm{T}(\mathrm{t}/\bar{\mathrm{t}})$ reweighting (orange solid line, labeled PH+P8+η_t). The hashed uncertainty bands correspond to the pre-fit systematic uncertainties and includes the statistical uncertainty of the data as well. The label 'p_T rew.' in the legend refers to the p_T reweighting procedure (detailed in section 7) used to reweight the $\mathrm{t\bar{t}}$ sample to NNLO in QCD.

near the production threshold of $\mathrm{t\bar{t}}$. The two lower panels of each plot in figure 3 show ratios of the various predictions to the data that more clearly demonstrate the improvement in modeling of the data when including contributions from the η_t state. Comparisons of different options on how to construct the combined signal model and generator choices are also included. Namely, data are compared in the upper panel to the case of POWHEGV2+PYTHIA8 not being reweighted to account for higher order corrections to the $p_\mathrm{T}(\mathrm{t}/\bar{\mathrm{t}})$ distribution (gray line in upper panel), or not including η_t (purple line in upper panel), or neither of them (red line in upper panel). The lower panel compares data to the nominal combined signal provided by POWHEGV2+PYTHIA8 (orange line in lower panel), to POWHEGV2+HERWIG++ (blue line in lower panel) and to MG5_aMC@NLO (FxFx)+PYTHIA8 (purple line in lower panel). The hashed band includes all systematic uncertainties described in section 7 for the combined signal model and all background contributions. The best overall modeling is given by the combined signal model of $\mathrm{t\bar{t}}+\eta_t$ and including $p_\mathrm{T}(\mathrm{t}/\bar{\mathrm{t}})$ and EWK corrections, while MG5_aMC@NLO (FxFx)+PYTHIA8 provides an improved modeling in $p_\mathrm{T}(\mathrm{t}/\bar{\mathrm{t}})$ but worse modeling in $m(\mathrm{t\bar{t}})$. However, it should be noted that the systematic uncertainties are at the pre-fit level, which means in particular that the η_t contribution has systematic uncertainties in excess of 50%.

Figure 4 shows MC modeling of the data in the analyzed phase space including the η_t state residing at lowest $m(\mathrm{t\bar{t}})$. Adequate modeling of the data can be seen even in the production threshold region below 400 GeV, which includes the η_t contribution. Systematic uncertainties were described earlier in more detail in section 7 and include (large) systematic uncertainties for the modeling of the η_t and the EWK corrections to the signal MC components. Within the selected phase space and including effects from $p_\mathrm{T}(\mathrm{t}/\bar{\mathrm{t}})$ reweighting and η_t, MG5_aMC@NLO (FxFx) provides a better description than

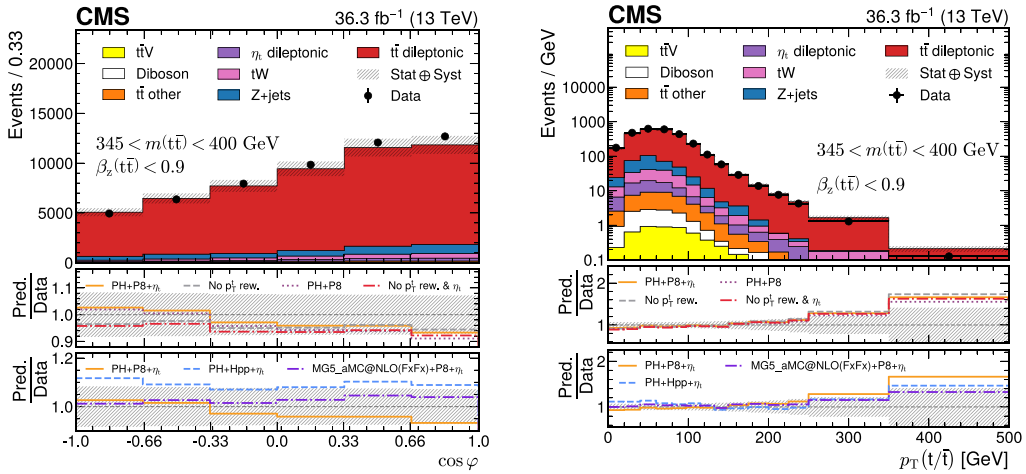

Figure 4. Reconstruction-level distributions of $\cos\varphi$ (left) and $p_T(t/\bar{t})$ (right) requiring $345 < m(t\bar{t}) < 400\,\text{GeV}$ and $\beta_z(t\bar{t}) < 0.9$. The lower panels on each figure show the same model comparison done in figure 3. The hashed uncertainty bands correspond to the pre-fit systematic uncertainties and includes the statistical uncertainty of the data as well. The label 'p_T rew.' in the legend refers to the p_T reweighting procedure (detailed in section 7) used to reweight the $t\bar{t}$ sample to NNLO in QCD.

the other event generators for both the $\cos\varphi$ and the $p_T(t/\bar{t})$ distributions.

9. Extraction of the entanglement proxy

The distribution of events at the reconstruction-level as a function of $\cos\varphi$ in the phase space of $345 < m(t\bar{t}) < 400\,\text{GeV}$ and $\beta_z(t\bar{t}) < 0.9$ is employed in a binned profile likelihood fit to measure the entanglement proxy D and to compare it with the boundary for entanglement. A single parameter of interest D is defined, which means that the combined $t\bar{t}$ and η_t signal are correlated in the likelihood fit, and only a single D is extracted at the end. We use templates with the expected yields as reported in table 1 as nominal input to the binned profile likelihood fit including shapes of all systematic uncertainties described in section 7 and define D as the single parameter of interest with an unconstrained shape prior. The profile likelihood fit is repeated while varying the entanglement proxy D and the minimum of the negative log likelihood is used to determine the best fit value for D. The uncertainty in D is determined from when the difference of the negative log likelihood values to the minimum crosses the values $-2\Delta\ln L = 1$.

In particular, templates are derived using the POWHEGV2 SM predictions implementing spin correlations for the $t\bar{t}$ component of the combined signal model including the assumed η_t contribution. We expect that mixtures of such a sample and a sample with purposely broken spin correlations can effectively model a continuous (linear) variation of the degree of entanglement between the top quarks by means of the entanglement proxy D. In order to have templates implementing an alternative value of the entanglement proxy D, we employ the noSC POWHEGV2 sample (including the assumed η_t noSC contribution) and 'mix' it in steps ranging from -100% to $+100\%$ with the combined signal model SM template. Figure 5 shows 'mixtures' obtained from three values (100% SC, 50%/50% noSC/SC, 100% noSC) as a function of $\cos\varphi$ at the detector level for the $t\bar{t}$ (left) and η_t (right) components of the combined signal model. The negative mixtures for $t\bar{t}$, shown in figure 5, are created mirroring the corresponding positive mixtures around the 100% SC mixture. The profile likelihood fit is prevented from fitting a negative noSC fraction for the η_t contribution as this would imply $D < -1$ and would have the consequence of predicting a portion of the differential cross section in $\cos\varphi$ to be negative, which is non-physical. Any particular mixture of combined SC and noSC signal corresponds to a certain value of D at the parton level by means of calculating a 2-bin asymmetry (A_D) with the combined signal model, consisting of $t\bar{t}$ and η_t. The value of

$$A_D = \frac{N(\cos\varphi > 0) - N(\cos\varphi < 0)}{N(\cos\varphi > 0) + N(\cos\varphi < 0)} \tag{7}$$

yields D as $-2A_D$, with N always being the sum of $t\bar{t}$ and η_t contributions.

The profile likelihood fit yields the value of the parameter of interest D directly at the parton level accounting for all detector effects due to acceptance, efficiency, and migration. The parton level corrected phase space is given by: $m(t\bar{t}) < 400\,\text{GeV}$ and $\beta_z(t\bar{t}) < 0.9$. These effects smear the definition of when top quark-antiquark states start becoming entangled at the detector level. We also include the shifts originating from the profile likelihood fit of all systematic uncertainties implemented as nuisance parameters and employ a scan of twice the negative log likelihood ($-2\Delta\ln L$) distribution of the parameter of interest D to measure its value and uncertainty.

The measurement of D via a binned profile likelihood fit and the scan of the $-2\Delta\ln L$ distribution are verified to be unbiased against different values of an injected D_{inject} at the parton level corresponding to top quarks with a varying degree of entanglement.

In order to determine whether top quarks are inseparable and consequently entangled, the measured value of D can be compared to the boundary for entanglement.

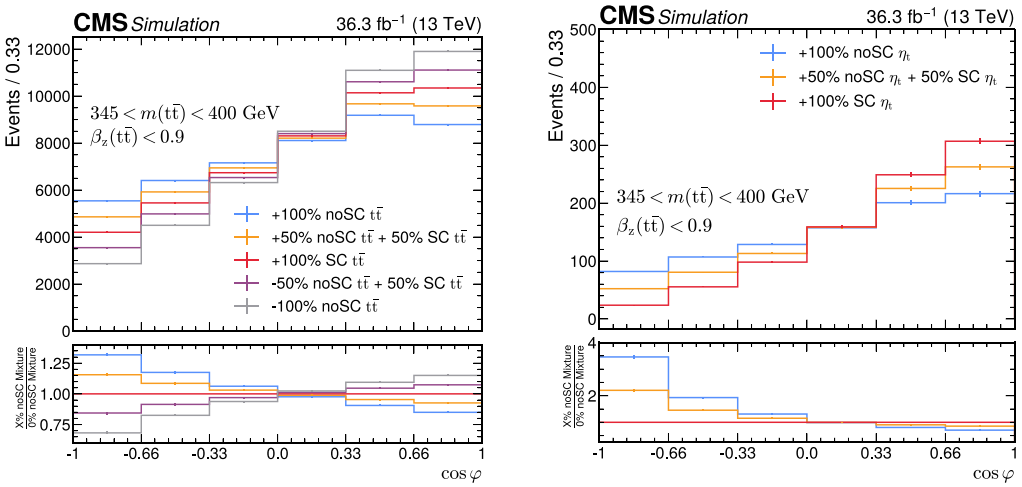

Figure 5. Reconstruction-level distribution of the combined $t\bar{t}+\eta_t$ signal model in mixtures of the noSC combined signal sample. Template variations as a function of $\cos\varphi$ requiring an $m(t\bar{t})$ of $345 < m(t\bar{t}) < 400\,\text{GeV}$ and $\beta_z(t\bar{t}) < 0.9$ are shown. The $t\bar{t}$ noSC and SC mixtures ranging from -100% to +100% noSC are shown on the left. The η_t noSC and SC mixtures ranging from zero noSC to +100% noSC are shown on the right.

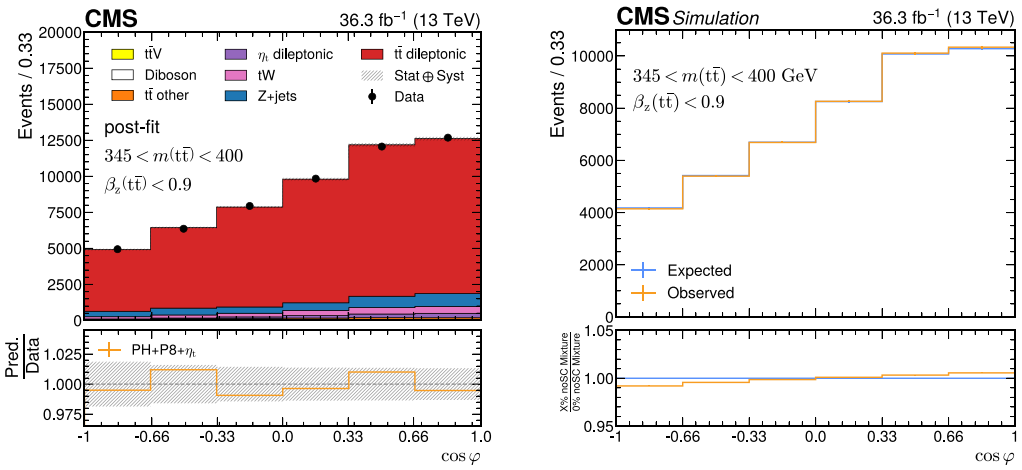

Figure 6. The post-fit detector-level distribution of $\cos\varphi$ requiring $345 < m(t\bar{t}) < 400\,\text{GeV}$, $\beta_z(t\bar{t}) < 0.9$, and including η_t in the fit, is shown on the left. The hashed band corresponds to the post-fit uncertainty and includes the statistical uncertainty of the data added in quadrature. The nominal combined signal model, POWHEG v2+PYTHIA 8+η_t, is labeled as PH+P8+η_t. The fitted noSC and SC mixture template for the combined signal model in the $\cos\varphi$ distribution is shown on the right.

10. Results

The result of the binned profile likelihood fit of the $\cos\varphi$ distribution is shown in figure 6 (left), and the data is well modeled by the combined signal model of $t\bar{t}+\eta_t$. Figure 6 (right) presents the expected and observed template of noSC and SC mixture and we observe a best fit mixture of the post-fit templates resulting in a $t\bar{t}$ contribution consistent with a 2.53% more spin correlated $t\bar{t}$ contribution when compared to the SM. The η_t contribution is consistent with 100% SC contribution, which is the expectation by the SM for the η_t contribution.

Table 3 provides the yields for each simulated sample and data at the pre-fit and post-fit level. The scan of the $-2\Delta\ln L$ distribution of the parameter of interest D is shown in figure 7 including the boundary for entanglement at $D = -1/3$.

The value of the entanglement proxy D in top quark events at the parton level is measured following the method described in the previous section and is available as a HEPData record [117]. For the phase space of $m(t\bar{t}) < 400\,\text{GeV}$ and $\beta_z(t\bar{t}) < 0.9$ at the parton level, an observed value of $D = -0.480^{+0.016}_{-0.017}(\text{stat})\,^{+0.020}_{-0.023}(\text{syst})$ is obtained in data, with an expected value of $D = -0.467^{+0.016}_{-0.017}(\text{stat})\,^{+0.021}_{-0.024}(\text{syst})$. With the boundary for entanglement at $-1/3$, this result corresponds to top quarks being entangled in this phase space with an observed (expected) significance of 5.1 (4.7) σ.

Removing the η_t contribution from the signal model and only considering the $t\bar{t}$ component as signal and re-measuring D in the same phase space as before yields an observed (expected) value of $D = -0.491^{+0.026}_{-0.025}(\text{tot.})$ ($D = -0.452^{+0.025}_{-0.026}(\text{tot.})$) at the parton level with an observed

Table 3. The number of predicted and observed events in the selected phase space, before the fit to the data (pre-fit) and with their best fit normalizations (post-fit). The uncertainties in the pre-fit and post-fit yields reflect total uncertanties but do not include correlations. The 'Only η_t' contribution is not added to the total MC prediction since it is included in the combined signal contribution.

Sample	Pre-fit	Post-fit
Signal ($t\bar{t}+\eta_t$)	$45\,800 \pm 1300$	$47\,560 \pm 380$
Z+jets	3560 ± 280	3490 ± 260
tW	1873 ± 72	1912 ± 64
$t\bar{t}$ other	572 ± 27	590 ± 22
Diboson	180 ± 12	185 ± 11
$t\bar{t}V$	100 ± 13	102 ± 14
Total MC	$52\,100 \pm 1600$	$53\,840 \pm 220$
Only η_t	890 ± 220	920 ± 190
Data	53 843	53 843

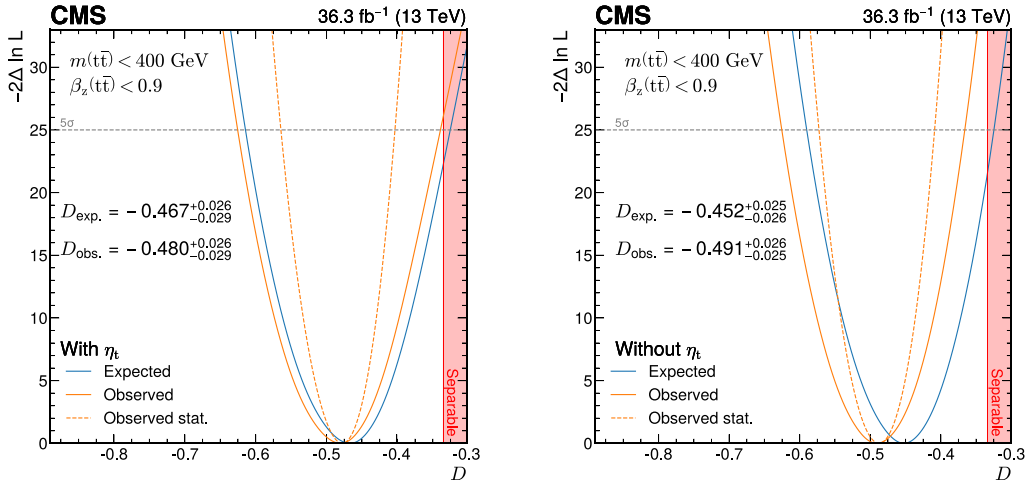

Figure 7. Result of the scan of the quantity $-2\Delta \ln L$ from a profile likelihood fit as a function of the parameter of interest D, when including (left) or excluding (right) the η_t contribution. Both results are at parton level and the relevant phase space is indicated in the figures itself. The region where the $t\bar{t}$ pairs become separable and not entangled ($D > -1/3$) is indicated by the shaded area.

(expected) significance of 6.3 (4.7) σ. Data are described better when the expected η_t contribution is included in the signal model.

Figure 8 shows the 20 leading nuisance parameters in the profile likelihood fit. The three leading uncertainties stem from the η_t signal contribution, the JES relative balance corrections, and the top quark p_T reweighting uncertainty. The latter and the uncertainty on EWK corrections are by construction one-sided.

Figure 9 shows the measured value of the entanglement proxy D, together with the predicted values from different MC event generators, in the relevant phase space, compared with the boundary for entanglement of top quarks. Overall, the data is in good agreement with the predictions from the three models, especially with the inclusion of the η_t contribution.

In addition, figure 9 provides the measured and predicted values of D in the same phase space but excluding the η_t contribution and only assuming the $t\bar{t}$ signal component. As a result, the measurement shows that MG5_aMC@NLO (FxFx) describes the data better, since the predictions by the other two models have some disagreement with the data at the level of one σ. While the observed values tend to be more negative, the predicted values from all three MCs become less negative owing to the missing effect of the η_t contribution. This difference in observed value originates from the inclusion of η_t causing a larger response in the shape of the $\cos\varphi$ distribution at the reconstruction level for a given change in the parton-level shape when compared with the no spin correlation mixing. Thus, for our specific technique of extracting the entanglement of $t\bar{t}$ pairs, an overestimation of the observed significance would be obtained, if η_t contributions were ignored. It is clearly visible that including the η_t signal component reduces the previously mentioned mild disagreement between data and simulation.

11. Summary

Entanglement is an intrinsic property of quantum mechanics and its measurement utilizes elementary particles to test quantum mechanics. Recently, the ATLAS Collaboration reported the first observation of entanglement in the top quark-antiquark ($t\bar{t}$) system [26] wih a result indicating a slight deviation from MC simulation.

The measurement of the entanglement of $t\bar{t}$ pairs performed with CMS data exploits the spin correlation variable

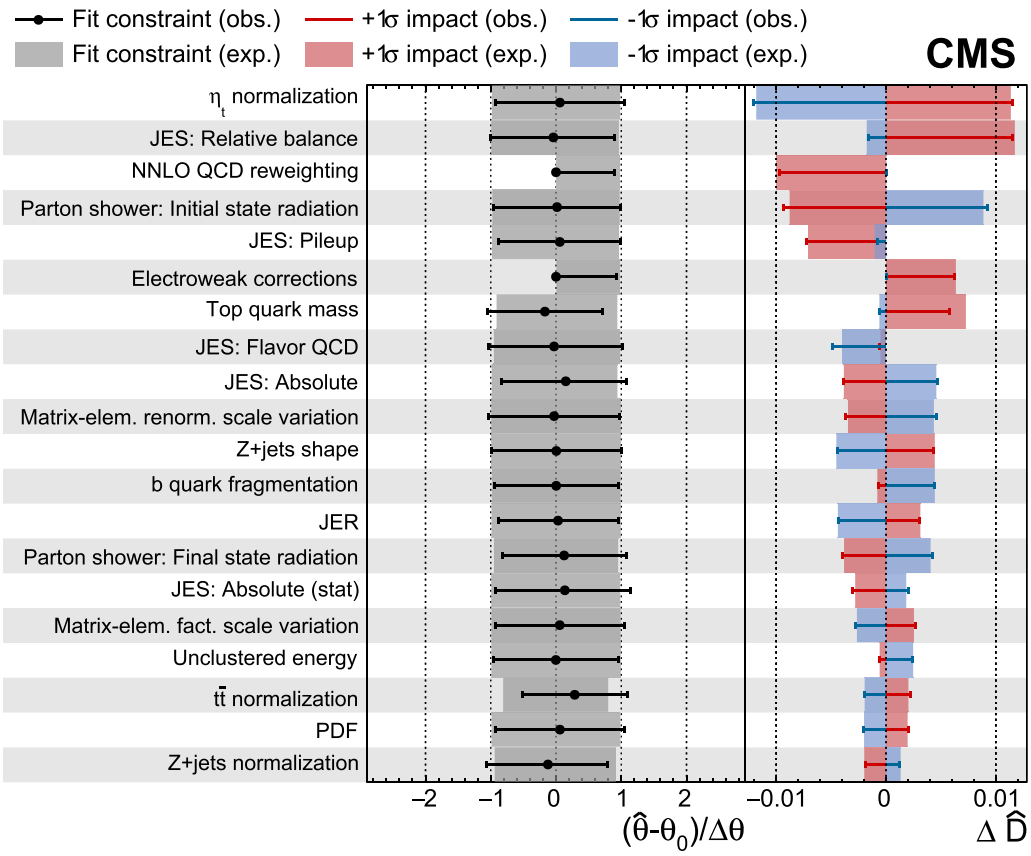

Figure 8. The left (right) column shows pulls (impacts) for the top 20 nuisance parameters affecting the measurement of the top quark entanglement. Pulls are calculated using pre- and post-fit values and uncertainties, while impacts are measured by shifting the nuisance parameter by $\pm 1\sigma$ and observing the change in D. The maximum likelihood estimate of the parameter of interest is denoted as $\hat{D}$. The NNLO QCD reweighting and EWK correction uncertainties are one-sided by construction, which can be seen by observing the one-sided pulls shown in the figure. For the NNLO QCD reweighting, we take the uncertainty as the full difference between applying this reweighting and not applying it, and provide it as the positive variation in the profile likelihood fit. For the EWK correction, the uncertainty is taken as the difference between applying the EWK corrections multiplicatively and additively and is provided as the positive variation in the profile likelihood fit.

D, which at the $\mathrm{t\bar{t}}$ production threshold, and in absence of BSM contributions, provides access to the full spin correlation information. This result contrasts with the ATLAS Collaboration's findings in several key ways. We measure entanglement at the parton level, whereas ATLAS reports their observable at the particle level. Additionally, our analysis is the first to consider non-relativistic bound-state effects in the production threshold by including the ground state of toponium, η_t, which were not included in the ATLAS result. Unlike ATLAS, the CMS result is derived from a binned likelihood fit to extract the entanglement proxy, rather than using a calibration curve.

The D variable represents an entanglement proxy, where a value of less than $-1/3$ signals the presence of entanglement. This proxy is measured using events containing two oppositely charged electrons or muons produced in pp collisions at a center-of-mass energy of 13 TeV. The modeling of the data is improved when including the additional predicted contribution of the ground state of toponium, η_t, and is utilized in a combined signal model of $\mathrm{t\bar{t}}+\eta_\mathrm{t}$ in the measurement. The extent to which $\mathrm{t\bar{t}}$ pairs are entangled is measured by means of a binned profile likelihood fit of the parameter of interest D directly from the distribution of $\cos\varphi$, where φ is the angle between the two charged decay leptons in their respective parent top quark rest frames. In the most sensitive kinematic phase space of the relative velocity between the lab and $\mathrm{t\bar{t}}$ reference frames $\beta_z(\mathrm{t\bar{t}}) < 0.9$, and of the invariant mass of the top quark pair $345 < m(\mathrm{t\bar{t}}) < 400\,\mathrm{GeV}$, the fit of the $\cos\varphi$ distribution yields an observed value of $D = -0.480^{+0.026}_{-0.029}$ and an expected value of $D = -0.467^{+0.026}_{-0.029}$ including the predicted η_t state.

This result has an observed (expected) significance of 5.1 (4.7) σ, corresponding to the observation of top quark entanglement. The measured value of D is in good agreement with the MC modeling in this phase space when including the expected η_t bound state contribution.

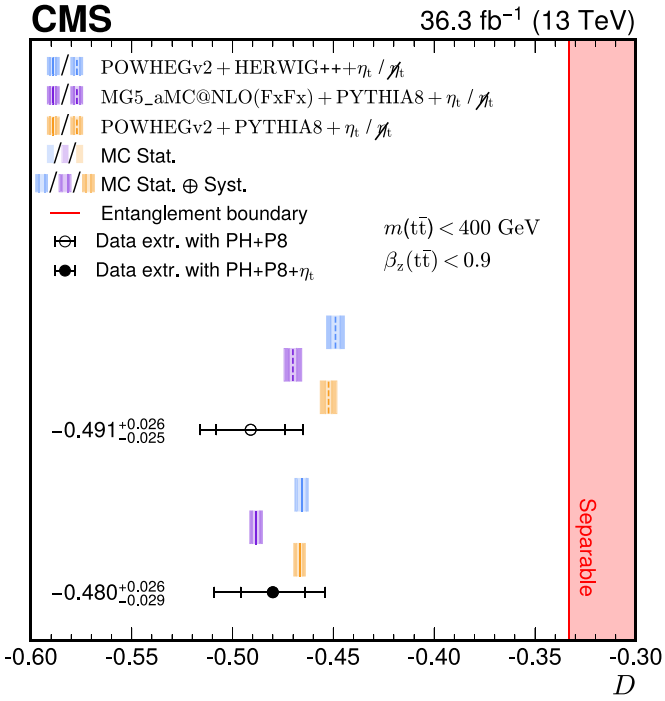

Figure 9. Summary of the measurement of the entanglement proxy D in data (black filled or open point) compared with MC predictions including (solid line) or not including (dashed line) contributions from the η_t state. The legend denotes MC predictions without the η_t state with a slash through η_t. Inner error bars represent the statistical uncertainty, while the outer error bars represent the total uncertainty for data. The statistical uncertainty in the MC predictions is denoted by the light shaded region and the total uncertainty, including scale and PDF uncertainties, is represented by the darker shaded region. The boundary for entanglement is indicated by the shaded region at $D = -1/3$.

Data availability statement

Release and preservation of data used by the CMS Collaboration as the basis for publications is guided by the CMS data preservation, re-use, and open access policy.

Acknowledgment

We congratulate our colleagues in the CERN accelerator departments for the excellent performance of the LHC and thank the technical and administrative staffs at CERN and at other CMS institutes for their contributions to the success of the CMS effort. In addition, we gratefully acknowledge the computing centers and personnel of the Worldwide LHC Computing Grid and other centers for delivering so effectively the computing infrastructure essential to our analyses. Finally, we acknowledge the enduring support for the construction and operation of the LHC, the CMS detector, and the supporting computing infrastructure provided by the following funding agencies: SC (Armenia), BMBWF and FWF (Austria); FNRS and FWO (Belgium); CNPq, CAPES, FAPERJ, FAPERGS, and FAPESP (Brazil); MES and BNSF (Bulgaria); CERN; CAS, MoST, and NSFC (China); MINCIENCIAS (Colombia); MSES and CSF (Croatia); RIF (Cyprus); SENESCYT (Ecuador); ERC PRG, RVTT3 and MoER TK202 (Estonia); Academy of Finland, MEC, and HIP (Finland); CEA and CNRS/IN2P3 (France); SRNSF (Georgia); BMBF, DFG, and HGF (Germany); GSRI (Greece); NKFIH (Hungary); DAE and DST (India); IPM (Iran); SFI (Ireland); INFN (Italy); MSIP and NRF (Republic of Korea); MES (Latvia); LMTLT (Lithuania); MOE and UM (Malaysia); BUAP, CINVESTAV, CONACYT, LNS, SEP, and UASLP-FAI (Mexico); MOS (Montenegro); MBIE (New Zealand); PAEC (Pakistan); MES and NSC (Poland); FCT (Portugal); MESTD (Serbia); MCIN/AEI and PCTI (Spain); MOSTR (Sri Lanka); Swiss Funding Agencies (Switzerland); MST (Taipei); MHESI and NSTDA (Thailand); TUBITAK and TENMAK (Turkey); NASU (Ukraine); STFC (United Kingdom); DOE and NSF (USA).

Individuals have received support from the Marie-Curie program and the European Research Council and Horizon 2020 Grant, Contract Nos. 675440, 724704, 752730, 758316, 765710, 824093, 101115353, 101002207, and COST Action CA16108 (European Union); the Leventis Foundation; the Alfred P. Sloan Foundation; the Alexander von Humboldt Foundation; the Science Committee, Project No. 22rl-037 (Armenia); the Belgian Federal Science Policy Office; the Fonds pour la Formation à la Recherche dans l'Industrie et dans l'Agriculture (FRIA-Belgium); the Agentschap voor Innovatie door Wetenschap en Technologie (IWT-Belgium); the F.R.S.-FNRS and FWO (Belgium) under the 'Excellence of Science—EOS'—be.h project n. 30820817; the Beijing Municipal Science & Technology Commission, No. Z191100007219010 and Fundamental Research Funds for the Central Universities (China); the

Ministry of Education, Youth and Sports (MEYS) of the Czech Republic; the Shota Rustaveli National Science Foundation, Grant FR-22-985 (Georgia); the Deutsche Forschungsgemeinschaft (DFG), under Germany's Excellence Strategy—EXC 2121 'Quantum Universe'—390833306, and under Project Number 400140256—GRK2497; the Hellenic Foundation for Research and Innovation (HFRI), Project Number 2288 (Greece); the Hungarian Academy of Sciences, the New National Excellence Program—ÚNKP, the NKFIH research Grants K 131991, K 133046, K 138136, K 143460, K 143477, K 146913, K 146914, K 147048, 2020-2.2.1-ED-2021-00181, and TKP2021-NKTA-64 (Hungary); the Council of Science and Industrial Research, India; ICSC—National Research Center for High Performance Computing, Big Data and Quantum Computing and FAIR—Future Artificial Intelligence Research, funded by the NextGenerationEU program (Italy); the Latvian Council of Science; the Ministry of Education and Science, Project No. 2022/WK/14, and the National Science Center, contracts Opus 2021/41/B/ST2/01369 and 2021/43/B/ST2/01552 (Poland); the Fundação para a Ciência e a Tecnologia, Grant CEECIND/01334/2018 (Portugal); the National Priorities Research Program by Qatar National Research Fund; MCIN/AEI/10.13039/501100011033, ERDF 'a way of making Europe', and the Programa Estatal de Fomento de la Investigación Científica y Técnica de Excelencia María de Maeztu, Grant MDM-2017-0765 and Programa Severo Ochoa del Principado de Asturias (Spain); the Chulalongkorn Academic into Its 2nd Century Project Advancement Project, and the National Science, Research and Innovation Fund via the Program Management Unit for Human Resources & Institutional Development, Research and Innovation, Grant B37G660013 (Thailand); the Kavli Foundation; the Nvidia Corporation; the SuperMicro Corporation; the Welch Foundation, Contract C-1845; and the Weston Havens Foundation (USA).

The CMS Collaboration

A Hayrapetyan, A Tumasyan[1]
Yerevan Physics Institute, Yerevan, Armenia

W Adam, J W Andrejkovic, T Bergauer, S Chatterjee, K Damanakis, M Dragicevic, A Hoang[2], P S Hussain, M Jeitler[3], N Krammer, A Li, D Liko, I Mikulec, J Schieck[3], R Schöfbeck, D Schwarz, M Sonawane, S Templ, W Waltenberger, C-E Wulz[3]
Institut für Hochenergiephysik, Vienna, Austria

T Janssen, T Van Laer, P Van Mechelen
Universiteit Antwerpen, Antwerpen, Belgium

N Breugelmans, J D'Hondt, S Dansana, A De Moor, M Delcourt, F Heyen, S Lowette, I Makarenko, D Müller, S Tavernier, M Tytgat[4], G P Van Onsem, S Van Putte, D Vannerom
Vrije Universiteit Brussel, Brussel, Belgium

B Bilin, B Clerbaux, A K Das, G De Lentdecker, H Evard, L Favart, P Gianneios, J Jaramillo, A Khalilzadeh, F A Khan, K Lee, M Mahdavikhorrami, A Malara, S Paredes, M A Shahzad, L Thomas, M Vanden Bemden, C Vander Velde, P Vanlaer
Université Libre de Bruxelles, Bruxelles, Belgium

M De Coen, D Dobur, G Gokbulut, Y Hong, J Knolle, L Lambrecht, D Marckx, K Mota Amarilo, A Samalan, K Skovpen, N Van Den Bossche, J van der Linden, L Wezenbeek
Ghent University, Ghent, Belgium

A Benecke, A Bethani, G Bruno, C Caputo, J De Favereau De Jeneret, C Delaere, I S Donertas, A Giammanco, A O Guzel, Sa. Jain, V Lemaitre, J Lidrych, P Mastrapasqua, T T Tran, S Wertz
Université Catholique de Louvain, Louvain-la-Neuve, Belgium

G A Alves, M Alves Gallo Pereira, E Coelho, G Correia Silva, C Hensel, T Menezes De Oliveira, C Mora Herrera[5], A Moraes, P Rebello Teles, M Soeiro, A Vilela Pereira[5]
Centro Brasileiro de Pesquisas Fisicas, Rio de Janeiro, Brazil

W L Aldá Júnior, M Barroso Ferreira Filho, H Brandao Malbouisson, W Carvalho, J Chinellato[6], E M Da Costa, G G Da Silveira[7], D De Jesus Damiao, S Fonseca De Souza, R Gomes De Souza, M Macedo, J Martins[8], L Mundim, H Nogima, J P Pinheiro, A Santoro, A Sznajder, M Thiel
Universidade do Estado do Rio de Janeiro, Rio de Janeiro, Brazil

C A Bernardes[7], L Calligaris, T R Fernandez Perez Tomei, E M Gregores, B Lopes Da Costa, I Maietto Silverio, P G Mercadante, S F Novaes, B Orzari, Sandra S Padula
Universidade Estadual Paulista, Universidade Federal do ABC, São Paulo, Brazil

A Aleksandrov, G Antchev, R Hadjiiska, P Iaydjiev, M Misheva, M Shopova, G Sultanov
Institute for Nuclear Research and Nuclear Energy, Bulgarian Academy of Sciences, Sofia, Bulgaria

A Dimitrov, L Litov, B Pavlov, P Petkov, A Petrov, E Shumka
University of Sofia, Sofia, Bulgaria

S Keshri, D Laroze, S Thakur

Instituto De Alta Investigación, Universidad de Tarapacá, Casilla 7 D, Arica, Chile

T Cheng, T Javaid, L Yuan

Beihang University, Beijing, People's Republic of China

Z Hu, Z Liang, J Liu, K Yi[9,10]
Department of Physics, Tsinghua University, Beijing, People's Republic of China

G M Chen[11], H S Chen[11], M Chen[11], F Iemmi, C H Jiang, A Kapoor[12], H Liao, Z-A Liu[13], R Sharma[14], J N Song[13], J Tao, C Wang[11], J Wang, Z Wang[11], H Zhang, J Zhao

Institute of High Energy Physics, Beijing, People's Republic of China

A Agapitos, Y Ban, S Deng, B Guo, C Jiang, A Levin, C Li, Q Li, Y Mao, S Qian, S J Qian, X Qin, X Sun, D Wang, H Yang, L Zhang, Y Zhao, C Zhou
State Key Laboratory of Nuclear Physics and Technology, Peking University, Beijing, People's Republic of China

S Yang
Guangdong Provincial Key Laboratory of Nuclear Science and Guangdong-Hong Kong Joint Laboratory of Quantum Matter, South China Normal University, Guangzhou, People's Republic of China

Z You
Sun Yat-Sen University, Guangzhou, People's Republic of China

K Jaffel, N Lu
University of Science and Technology of China, Hefei, People's Republic of China

G Bauer[15], B Li, J Zhang
Nanjing Normal University, Nanjing, People's Republic of China

X Gao[16], Y Li
Institute of Modern Physics and Key Laboratory of Nuclear Physics and Ion-beam Application (MOE) - Fudan University, Shanghai, People's Republic of China

Z Lin, C Lu, M Xiao
Zhejiang University, Hangzhou, Zhejiang, People's Republic of China

C Avila, D A Barbosa Trujillo, A Cabrera, C Florez, J Fraga, J A Reyes Vega
Universidad de Los Andes, Bogota, Colombia

F Ramirez, C Rendón, M Rodriguez, A A Ruales Barbosa, J D Ruiz Alvarez
Universidad de Antioquia, Medellin, Colombia

D Giljanovic, N Godinovic, D Lelas, A Sculac
University of Split, Faculty of Electrical Engineering, Mechanical Engineering and Naval Architecture, Split, Croatia

M Kovac, A Petkovic, T Sculac
University of Split, Faculty of Science, Split, Croatia

P Bargassa, V Brigljevic, B K Chitroda, D Ferencek, K Jakovcic, S Mishra, A Starodumov[17], T Susa
Institute Rudjer Boskovic, Zagreb, Croatia

A Attikis, K Christoforou, A Hadjiagapiou, C Leonidou, J Mousa, C Nicolaou, L Paizanos, F Ptochos, P A Razis, H Rykaczewski, H Saka, A Stepennov
University of Cyprus, Nicosia, Cyprus

M Finger, M Finger Jr, A Kveton
Charles University, Prague, Czech Republic

E Carrera Jarrin
Universidad San Francisco de Quito, Quito, Ecuador

Y Assran[18,19], B El-mahdy, S Elgammal[19]
Academy of Scientific Research and Technology of the Arab Republic of Egypt, Egyptian Network of High Energy Physics, Cairo, Egypt

M Abdullah Al-Mashad, M A Mahmoud
Center for High Energy Physics (CHEP-FU), Fayoum University, El-Fayoum, Egypt

K Ehataht, M Kadastik, T Lange, S Nandan, C Nielsen, J Pata, M Raidal, L Tani, C Veelken
National Institute of Chemical Physics and Biophysics, Tallinn, Estonia

H Kirschenmann, K Osterberg, M Voutilainen
Department of Physics, University of Helsinki, Helsinki, Finland

S Bharthuar, N Bin Norjoharuddeen, E Brücken, F Garcia, P Inkaew, K T S Kallonen, T Lampén, K Lassila-Perini, S Lehti, T Lindén, L Martikainen, M Myllymäki, M M Rantanen, H Siikonen, J Tuominiemi
Helsinki Institute of Physics, Helsinki, Finland

P Luukka, H Petrow
Lappeenranta-Lahti University of Technology, Lappeenranta, Finland

M Besancon, F Couderc, M Dejardin, D Denegri, J L Faure, F Ferri, S Ganjour, P Gras, G Hamel de

Monchenault, M Kumar, V Lohezic, J Malcles, F Orlandi, L Portales, A Rosowsky, M Ö. Sahin, A Savoy-Navarro[20], P Simkina, M Titov, M Tornago
IRFU, CEA, Université Paris-Saclay, Gif-sur-Yvette, France

F Beaudette, G Boldrini, P Busson, A Cappati, C Charlot, M Chiusi, F Damas, O Davignon, A De Wit, I T Ehle, B A Fontana Santos Alves, S Ghosh, A Gilbert, R Granier de Cassagnac, A Hakimi, B Harikrishnan, L Kalipoliti, G Liu, M Nguyen, C Ochando, R Salerno, J B Sauvan, Y Sirois, L Urda Gómez, E Vernazza, A Zabi, A Zghiche
Laboratoire Leprince-Ringuet, CNRS/IN2P3, Ecole Polytechnique, Institut Polytechnique de Paris, Palaiseau, France

J-L Agram[21], J Andrea, D Apparu, D Bloch, J-M Brom, E C Chabert, C Collard, S Falke, U Goerlach, R Haeberle, A-C Le Bihan, M Meena, O Poncet, G Saha, M A Sessini, P Van Hove, P Vaucelle
Université de Strasbourg, CNRS, IPHC UMR 7178, Strasbourg, France

A Di Florio
Centre de Calcul de l'Institut National de Physique Nucleaire et de Physique des Particules, CNRS/IN2P3, Villeurbanne, France

D Amram, S Beauceron, B Blancon, G Boudoul, N Chanon, D Contardo, P Depasse, C Dozen[22], H El Mamouni, J Fay, S Gascon, M Gouzevitch, C Greenberg, G Grenier, B Ille, E Jourd'huy, I B Laktineh, M Lethuillier, L Mirabito, S Perries, A Purohit, M Vander Donckt, P Verdier, J Xiao
Institut de Physique des 2 Infinis de Lyon (IP2I), Villeurbanne, France

A Khvedelidze[17], I Lomidze, Z Tsamalaidze[17]
Georgian Technical University, Tbilisi, Georgia

V Botta, S Consuegra Rodríguez, L Feld, K Klein, M Lipinski, D Meuser, A Pauls, D Pérez Adán, N Röwert, M Teroerde
RWTH Aachen University, I. Physikalisches Institut, Aachen, Germany

S Diekmann, A Dodonova, N Eich, D Eliseev, F Engelke, J Erdmann, M Erdmann, P Fackeldey, B Fischer, T Hebbeker, K Hoepfner, F Ivone, A Jung, M Y Lee, F Mausolf, M Merschmeyer, A Meyer, S Mukherjee, D Noll, F Nowotny, A Pozdnyakov, Y Rath, W Redjeb, F Rehm, H Reithler, V Sarkisovi, A Schmidt, A Sharma, J L Spah, A Stein, F Torres Da Silva De Araujo[23], S Wiedenbeck, S Zaleski
RWTH Aachen University, III. Physikalisches Institut A, Aachen, Germany

C Dziwok, G Flügge, T Kress, A Nowack, O Pooth, A Stahl, T Ziemons, A Zotz
RWTH Aachen University, III. Physikalisches Institut B, Aachen, Germany

H Aarup Petersen, M Aldaya Martin, J Alimena, S Amoroso, Y An, J Bach, S Baxter, M Bayatmakou, H Becerril Gonzalez, O Behnke, A Belvedere, F Blekman[24], K Borras[25], A Campbell, A Cardini, C Cheng, F Colombina, M De Silva, G Eckerlin, D Eckstein, L I Estevez Banos, O Filatov, E Gallo[24], A Geiser, V Guglielmi, M Guthoff, A Hinzmann, L Jeppe, B Kaech, M Kasemann, C Kleinwort, R Kogler, M Komm, D Krücker, W Lange, D Leyva Pernia, K Lipka[26], W Lohmann[27], F Lorkowski, R Mankel, I-A Melzer-Pellmann, M Mendizabal Morentin, A B Meyer, G Milella, K Moral Figueroa, A Mussgiller, L P Nair, J Niedziela, A Nürnberg, Y Otarid, J Park, E Ranken, A Raspereza, D Rastorguev, J Rübenach, L Rygaard, A Saggio, M Scham[28,25], S Schnake[25], P Schütze, C Schwanenberger[24], D Selivanova, K Sharko, M Shchedrolosiev, D Stafford, F Vazzoler, A Ventura Barroso, R Walsh, D Wang, Q Wang, Y Wen, K Wichmann, L Wiens[25], C Wissing, Y Yang, A Zimermmane Castro Santos
Deutsches Elektronen-Synchrotron, Hamburg, Germany

A Albrecht, S Albrecht, M Antonello, S Bein, L Benato, S Bollweg, M Bonanomi, P Connor, K El Morabit, Y Fischer, E Garutti, A Grohsjean, J Haller, H R Jabusch, G Kasieczka, P Keicher, R Klanner, W Korcari, T Kramer, C C Kuo, V Kutzner, F Labe, J Lange, A Lobanov, C Matthies, L Moureaux, M Mrowietz, A Nigamova, Y Nissan, A Paasch, K J Pena Rodriguez, T Quadfasel, B Raciti, M Rieger, D Savoiu, J Schindler, P Schleper, M Schröder, J Schwandt, M Sommerhalder, H Stadie, G Steinbrück, A Tews, M Wolf
University of Hamburg, Hamburg, Germany

S Brommer, M Burkart, E Butz, T Chwalek, A Dierlamm, A Droll, U Elicabuk, N Faltermann, M Giffels, A Gottmann, F Hartmann[29], R Hofsaess, M Horzela, U Husemann, J Kieseler, M Klute, R Koppenhöfer, J M Lawhorn, M Link, A Lintuluoto, B Maier, S Maier, S Mitra, M Mormile, Th Müller, M Neukum, M Oh, E Pfeffer, M Presilla, G Quast, K Rabbertz, B Regnery, N Shadskiy, I Shvetsov, H J Simonis, L Sowa, L Stockmeier, K Tauqeer, M Toms, N Trevisani, R F Von Cube, M Wassmer, S Wieland, F Wittig, R Wolf, X Zuo

Karlsruher Institut fuer Technologie, Karlsruhe, Germany

G Anagnostou, G Daskalakis, A Kyriakis, A Papadopoulos[29], A Stakia
Institute of Nuclear and Particle Physics (INPP), NCSR Demokritos, Aghia Paraskevi, Greece

P Kontaxakis, G Melachroinos, Z Painesis, I Papavergou, I Paraskevas, N Saoulidou, K Theofilatos, E Tziaferi, K Vellidis, I Zisopoulos

National and Kapodistrian University of Athens, Athens, Greece

G Bakas, T Chatzistavrou, G Karapostoli, K Kousouris, I Papakrivopoulos, E Siamarkou, G Tsipolitis, A Zacharopoulou
National Technical University of Athens, Athens, Greece

K Adamidis, I Bestintzanos, I Evangelou, C Foudas, C Kamtsikis, P Katsoulis, P Kokkas, P G Kosmoglou Kioseoglou, N Manthos, I Papadopoulos, J Strologas
University of Ioánnina, Ioánnina, Greece

C Hajdu, D Horvath[30,31], K Márton, A J Rádl[32], F Sikler, V Veszpremi
HUN-REN Wigner Research Centre for Physics, Budapest, Hungary

M Csanád, K Farkas, A Fehérkuti[33], M M A Gadallah[34], Á. Kadlecsik, P Major, G Pásztor, G I Veres
MTA-ELTE Lendület CMS Particle and Nuclear Physics Group, Eötvös Loránd University, Budapest, Hungary

B Ujvari, G Zilizi
Faculty of Informatics, University of Debrecen, Debrecen, Hungary

G Bencze, S Czellar, J Molnar, Z Szillasi
Institute of Nuclear Research ATOMKI, Debrecen, Hungary

F Nemes[33], T Novak
Karoly Robert Campus, MATE Institute of Technology, Gyongyos, Hungary

S Bansal, S B Beri, V Bhatnagar, G Chaudhary, S Chauhan, N Dhingra[35], A Kaur, A Kaur, H Kaur, M Kaur, S Kumar, K Sandeep, T Sheokand, J B Singh, A Singla
Panjab University, Chandigarh, India

A Ahmed, A Bhardwaj, A Chhetri, B C Choudhary, A Kumar, A Kumar, M Naimuddin, K Ranjan, M K Saini, S Saumya
University of Delhi, Delhi, India

S Baradia, S Barman[36], S Bhattacharya, S Das Gupta, S Dutta, S Dutta, S Sarkar
Saha Institute of Nuclear Physics, HBNI, Kolkata, India

M M Ameen, P K Behera, S C Behera, S Chatterjee, G Dash, P Jana, P Kalbhor, S Kamble, J R Komaragiri[37], D Kumar[37], P R Pujahari, N R Saha, A Sharma, A K Sikdar, R K Singh, P Verma, S Verma, A Vijay

Indian Institute of Technology Madras, Madras, India

S Dugad, G B Mohanty, B Parida, M Shelake, P Suryadevara
Tata Institute of Fundamental Research-A, Mumbai, India

A Bala, S Banerjee, R M Chatterjee, M Guchait, Sh Jain, A Jaiswal, S Kumar, G Majumder, K Mazumdar, S Parolia, A Thachayath
Tata Institute of Fundamental Research-B, Mumbai, India

S Bahinipati[38], C Kar, D Maity[39], P Mal, T Mishra, V K Muraleedharan Nair Bindhu[39], K Naskar[39], A Nayak[39], S Nayak, K Pal, P Sadangi, S K Swain, S Varghese[39], D Vats[39]
National Institute of Science Education and Research, An OCC of Homi Bhabha National Institute, Bhubaneswar, Odisha, India

S Acharya[40], A Alpana, S Dube, B Gomber[40], P Hazarika, B Kansal, A Laha, B Sahu[40], S Sharma, K Y Vaish
Indian Institute of Science Education and Research (IISER), Pune, India

H Bakhshiansohi[41], A Jafari[42], M Zeinali[43]
Isfahan University of Technology, Isfahan, Iran

S Bashiri, S Chenarani[44], S M Etesami, Y Hosseini, M Khakzad, E Khazaie[45], M Mohammadi Najafabadi, S Tizchang[46]
Institute for Research in Fundamental Sciences (IPM), Tehran, Iran

M Felcini, M Grunewald
University College Dublin, Dublin, Ireland

M Abbrescia[a,b], A Colaleo[a,b], D Creanza[a,c], B D'Anzi[a,b], N De Filippis[a,c], M De Palma[a,b], W Elmetenawee[a,b,47], L Fiore[a], G Iaselli[a,c], L Longo[a], M Louka[a,b], G Maggi[a,c], M Maggi[a], I Margjeka[a], V Mastrapasqua[a,b], S My[a,b], S Nuzzo[a,b], A Pellecchia[a,b], A Pompili[a,b], G Pugliese[a,c], R Radogna[a,b], D Ramos[a], A Ranieri[a], L Silvestris[a],

F M Simone[a,c], Ü. Sözbilir[a], A Stamerra[a,b], D Troiano[a,b], R Venditti[a,b], P Verwilligen[a], A Zaza[a,b]

INFN Sezione di Bari[a], Università di Bari[b], Politecnico di Bari[c], Bari, Italy

G Abbiendi[a], C Battilana[a,b], D Bonacorsi[a,b], P Capiluppi[a,b], A Castro[†,a,b], F R Cavallo[a], M Cuffiani[a,b], G M Dallavalle[a], T Diotalevi[a,b], F Fabbri[a], A Fanfani[a,b], D Fasanella[a], P Giacomelli[a], L Giommi[a,b], C Grandi[a], L Guiducci[a,b], S Lo Meo[a,48], M Lorusso[a,b], L Lunerti[a], S Marcellini[a], G Masetti[a], F L Navarria[a,b], G Paggi[a,b], A Perrotta[a], F Primavera[a,b], A M Rossi[a,b], S Rossi Tisbeni[a,b], T Rovelli[a,b], G P Siroli[a,b]

INFN Sezione di Bologna[a], Università di Bologna[b], Bologna, Italy

S Costa[a,b,49], A Di Mattia[a], A Lapertosa[a], R Potenza[a,b], A Tricomi[a,b,49], C Tuve[a,b]

INFN Sezione di Catania[a], Università di Catania[b], Catania, Italy

P Assiouras[a], G Barbagli[a], G Bardelli[a,b], B Camaiani[a,b], A Cassese[a], R Ceccarelli[a], V Ciulli[a,b], C Civinini[a], R D'Alessandro[a,b], E Focardi[a,b], T Kello[a], G Latino[a,b], P Lenzi[a,b], M Lizzo[a], M Meschini[a], S Paoletti[a], A Papanastassiou[a,b], G Sguazzoni[a], L Viliani[a]

INFN Sezione di Firenze[a], Università di Firenze[b], Firenze, Italy

L Benussi, S Bianco, S Meola[50], D Piccolo

INFN Laboratori Nazionali di Frascati, Frascati, Italy

P Chatagnon[a], F Ferro[a], E Robutti[a], S Tosi[a,b]

INFN Sezione di Genova[a], Università di Genova[b], Genova, Italy

A Benaglia[a], F Brivio[a], F Cetorelli[a,b], F De Guio[a,b], M E Dinardo[a,b], P Dini[a], S Gennai[a], R Gerosa[a,b], A Ghezzi[a,b], P Govoni[a,b], L Guzzi[a], M T Lucchini[a,b], M Malberti[a], S Malvezzi[a], A Massironi[a], D Menasce[a], L Moroni[a], M Paganoni[a,b], S Palluotto[a,b], D Pedrini[a], A Perego[a,b], B S Pinolini[a], G Pizzati[a,b], S Ragazzi[a,b], T Tabarelli de Fatis[a,b]

INFN Sezione di Milano-Bicocca[a], Università di Milano-Bicocca[b], Milano, Italy

S Buontempo[a], A Cagnotta[a,b], F Carnevali[a,b], N Cavallo[a,c], F Fabozzi[a,c], A O M Iorio[a,b], L Lista[a,b,51], P Paolucci[a,29], B Rossi[a]

INFN Sezione di Napoli[a], Università di Napoli 'Federico II'[b], Napoli, Italy; Università della Basilicata[c], Potenza, Italy; Scuola Superiore Meridionale (SSM)[d], Napoli, Italy

R Ardino[a], P Azzi[a], N Bacchetta[a,52], P Bortignon[a], G Bortolato[a,b], A Bragagnolo[a,b], A C M Bulla[a], R Carlin[a,b], P Checchia[a], T Dorigo[a], U Gasparini[a,b], F Gonella[a], A Gozzelino[a], E Lusiani[a], M Margoni[a,b], A T Meneguzzo[a,b], M Migliorini[a,b], J Pazzini[a,b], P Ronchese[a,b], R Rossin[a,b], F Simonetto[a,b], M Tosi[a,b], A Triossi[a,b], S Ventura[a], M Zanetti[a,b], P Zotto[a,b], A Zucchetta[a,b], G Zumerle[a,b]

INFN Sezione di Padova[a], Università di Padova[b], Padova, Italy; Università di Trento[c], Trento, Italy

C Aimè[a], A Braghieri[a], S Calzaferri[a], D Fiorina[a], P Montagna[a,b], V Re[a], C Riccardi[a,b], P Salvini[a], I Vai[a,b], P Vitulo[a,b]

INFN Sezione di Pavia[a], Università di Pavia[b], Pavia, Italy

S Ajmal[a,b], M E Ascioti[a,b], G M Bilei[a], C Carrivale[a,b], D Ciangottini[a,b], L Fanò[a,b], M Magherini[a,b], V Mariani[a,b], M Menichelli[a], F Moscatelli[a,53], A Rossi[a,b], A Santocchia[a,b], D Spiga[a], T Tedeschi[a,b]

INFN Sezione di Perugia[a], Università di Perugia[b], Perugia, Italy

C A Alexe[a,c], P Asenov[a,b], P Azzurri[a], G Bagliesi[a], R Bhattacharya[a], L Bianchini[a,b], T Boccali[a], E Bossini[a], D Bruschini[a,c], R Castaldi[a], M A Ciocci[a,b], M Cipriani[a,b], V D'Amante[a,d], R Dell'Orso[a], S Donato[a], A Giassi[a], F Ligabue[a,c], A C Marini[a], D Matos Figueiredo[a], A Messineo[a,b], M Musich[a,b], F Palla[a], A Rizzi[a,b], G Rolandi[a,c], S Roy Chowdhury[a], T Sarkar[a], A Scribano[a], P Spagnolo[a], R Tenchini[a], G Tonelli[a,b], N Turini[a,d], F Vaselli[a,c], A Venturi[a], P G Verdini[a]

INFN Sezione di Pisa[a], Università di Pisa[b], Scuola Normale Superiore di Pisa[c], Pisa, Italy; Università di Siena[d], Siena, Italy

C Baldenegro Barrera[a,b], P Barria[a], C Basile[a,b], M Campana[a,b], F Cavallari[a], L Cunqueiro Mendez[a,b], D Del Re[a,b], E Di Marco[a,b], M Diemoz[a], F Errico[a,b], E Longo[a,b], J Mijuskovic[a,b], G Organtini[a,b], F Pandolfi[a], R Paramatti[a,b], C Quaranta[a,b], S Rahatlou[a,b], C Rovelli[a], F Santanastasio[a,b], L Soffi[a]

INFN Sezione di Roma[a], Sapienza Università di Roma[b], Roma, Italy

N Amapane[a,b], R Arcidiacono[a,c], S Argiro[a,b], M Arneodo[a,c], N Bartosik[a], R Bellan[a,b], A Bellora[a,b], C Biino[a], C Borca[a,b], N Cartiglia[a], M Costa[a,b], R Covarelli[a,b], N Demaria[a], L Finco[a], M Grippo[a,b],

B Kiani[a,b], F Legger[a], F Luongo[a,b], C Mariotti[a], L Markovic[a,b], S Maselli[a], A Mecca[a,b], L Menzio[a,b], P Meridiani[a], E Migliore[a,b], M Monteno[a], R Mulargia[a], M M Obertino[a,b], G Ortona[a], L Pacher[a,b], N Pastrone[a], M Pelliccioni[a], M Ruspa[a,c], F Siviero[a,b], V Sola[a,b], A Solano[a,b], A Staiano[a], C Tarricone[a,b], D Trocino[a], G Umoret[a,b], R White[a,b]
INFN Sezione di Torino[a], Università di Torino[b], Torino, Italy; Università del Piemonte Orientale[c], Novara, Italy

J Babbar[a,b], S Belforte[a], V Candelise[a,b], M Casarsa[a], F Cossutti[a], K De Leo[a], G Della Ricca[a,b]
INFN Sezione di Trieste[a], Università di Trieste[b], Trieste, Italy

S Dogra, J Hong, C Huh, B Kim, J Kim, D Lee, H Lee, S W Lee, C S Moon, Y D Oh, M S Ryu, S Sekmen, B Tae, Y C Yang
Kyungpook National University, Daegu, Republic of Korea

M S Kim

Department of Mathematics and Physics - GWNU, Gangneung, Republic of Korea

G Bak, P Gwak, H Kim, D H Moon

Chonnam National University, Institute for Universe and Elementary Particles, Kwangju, Republic of Korea

E Asilar, J Choi, D Kim, T J Kim, J A Merlin, Y Ryou
Hanyang University, Seoul, Republic of Korea

S Choi, S Han, B Hong, K Lee, K S Lee, S Lee, J Yoo
Korea University, Seoul, Republic of Korea

J Goh, S Yang
Kyung Hee University, Department of Physics, Seoul, Republic of Korea

H S Kim, Y Kim, S Lee
Sejong University, Seoul, Republic of Korea

J Almond, J H Bhyun, J Choi, J Choi, W Jun, J Kim, S Ko, H Kwon, H Lee, J Lee, J Lee, B H Oh, S B Oh, H Seo, U K Yang, I Yoon
Seoul National University, Seoul, Republic of Korea

W Jang, D Y Kang, Y Kang, S Kim, B Ko, J S H Lee, Y Lee, I C Park, Y Roh, I J Watson
University of Seoul, Seoul, Republic of Korea

S Ha, H D Yoo
Yonsei University, Department of Physics, Seoul, Republic of Korea

M Choi, M R Kim, H Lee, Y Lee, I Yu
Sungkyunkwan University, Suwon, Republic of Korea

T Beyrouthy, Y Gharbia
College of Engineering and Technology, American University of the Middle East (AUM), Dasman, Kuwait

K Dreimanis, A Gaile, C Munoz Diaz, D Osite, G Pikurs, A Potrebko, M Seidel, D Sidiropoulos Kontos
Riga Technical University, Riga, Latvia

N R Strautnieks

University of Latvia (LU), Riga, Latvia

M Ambrozas, A Juodagalvis, A Rinkevicius, G Tamulaitis
Vilnius University, Vilnius, Lithuania

I Yusuff[54], Z Zolkapli

National Centre for Particle Physics, Universiti Malaya, Kuala Lumpur, Malaysia

J F Benitez, A Castaneda Hernandez, H A Encinas Acosta, L G Gallegos Maríñez, M León Coello, J A Murillo Quijada, A Sehrawat, L Valencia Palomo
Universidad de Sonora (UNISON), Hermosillo, Mexico

G Ayala, H Castilla-Valdez, H Crotte Ledesma, E De La Cruz-Burelo, I Heredia-De La Cruz[55], R Lopez-Fernandez, J Mejia Guisao, C A Mondragon Herrera, A Sánchez Hernández
Centro de Investigacion y de Estudios Avanzados del IPN, Mexico City, Mexico

C Oropeza Barrera, D L Ramirez Guadarrama, M Ramírez García
Universidad Iberoamericana, Mexico City, Mexico

I Bautista, I Pedraza, H A Salazar Ibarguen, C Uribe Estrada
Benemerita Universidad Autonoma de Puebla, Puebla, Mexico

I Bubanja, N Raicevic
University of Montenegro, Podgorica, Montenegro

P H Butler
University of Canterbury, Christchurch, New Zealand

A Ahmad, M I Asghar, A Awais, M I M Awan, H R Hoorani, W A Khan
National Centre for Physics, Quaid-I-Azam University, Islamabad, Pakistan

V Avati, L Grzanka, M Malawski
AGH University of Krakow, Faculty of Computer Science, Electronics and Telecommunications, Krakow, Poland

H Bialkowska, M Bluj, M Górski, M Kazana, M Szleper, P Zalewski
National Centre for Nuclear Research, Swierk, Poland

K Bunkowski, K Doroba, A Kalinowski, M Konecki, J Krolikowski, A Muhammad
Institute of Experimental Physics, Faculty of Physics, University of Warsaw, Warsaw, Poland

K Pozniak, W Zabolotny

Warsaw University of Technology, Warsaw, Poland

M Araujo, D Bastos, C Beirão Da Cruz E Silva, A Boletti, M Bozzo, T Camporesi, G Da Molin, P Faccioli, M Gallinaro, J Hollar, N Leonardo, G B Marozzo, T Niknejad, A Petrilli, M Pisano, J Seixas, J Varela, J W Wulff

Laboratório de Instrumentação e Física Experimental de Partículas, Lisboa, Portugal

P Adzic, P Milenovic
Faculty of Physics, University of Belgrade, Belgrade, Serbia

M Dordevic, J Milosevic, V Rekovic
VINCA Institute of Nuclear Sciences, University of Belgrade, Belgrade, Serbia

J Alcaraz Maestre, Cristina F Bedoya, Oliver M Carretero, M Cepeda, M Cerrada, N Colino, B De La Cruz, A Delgado Peris, A Escalante Del Valle, D Fernández Del Val, J P Fernández Ramos, J Flix, M C Fouz, O Gonzalez Lopez, S Goy Lopez, J M Hernandez, M I Josa, E Martin Viscasillas, D Moran, C M Morcillo Perez, Á. Navarro Tobar, C Perez Dengra, A Pérez-Calero Yzquierdo, J Puerta Pelayo, I Redondo, S Sánchez Navas, J Sastre, J Vazquez Escobar
Centro de Investigaciones Energéticas Medioambientales y Tecnológicas (CIEMAT), Madrid, Spain

J F de Trocóniz
Universidad Autónoma de Madrid, Madrid, Spain

B Alvarez Gonzalez, J Cuevas, J Fernandez Menendez, S Folgueras, I Gonzalez Caballero, J R González Fernández, P Leguina, E Palencia Cortezon, J Prado Pico, C Ramón Álvarez, V Rodríguez Bouza, A Soto Rodríguez, A Trapote, C Vico Villalba, P Vischia
Universidad de Oviedo, Instituto Universitario de Ciencias y Tecnologías Espaciales de Asturias (ICTEA), Oviedo, Spain

S Bhowmik, S Blanco Fernández, J A Brochero Cifuentes, I J Cabrillo, A Calderon, J Duarte Campderros, M Fernandez, G Gomez, C Lasaosa García, R Lopez Ruiz, C Martinez Rivero, P Martinez Ruiz del Arbol, F Matorras, P Matorras Cuevas, E Navarrete Ramos, J Piedra Gomez, L Scodellaro, I Vila, J M Vizan Garcia
Instituto de Física de Cantabria (IFCA), CSIC-Universidad de Cantabria, Santander, Spain

B Kailasapathy[56], D D C Wickramarathna
University of Colombo, Colombo, Sri Lanka

W G D Dharmaratna[57], K Liyanage, N Perera
University of Ruhuna, Department of Physics, Matara, Sri Lanka

D Abbaneo, C Amendola, E Auffray, G Auzinger, J Baechler, D Barney, A Bermúdez Martínez, M Bianco, A A Bin Anuar, A Bocci, L Borgonovi, C Botta, E Brondolin, C Caillol, G Cerminara, N Chernyavskaya, D d'Enterria, A Dabrowski, A David, A De Roeck, M M Defranchis, M Deile, M Dobson, G Franzoni, W Funk, S Giani, D Gigi, K Gill, F Glege, J Hegeman, J K Heikkilä, B Huber, V Innocente, T James, P Janot, O Kaluzinska, O Karacheban[27], S Laurila, P Lecoq, E Leutgeb, C Lourenço, L Malgeri, M Mannelli, M Matthewman, A Mehta, F Meijers, S Mersi, E Meschi, V Milosevic, F Monti, F Moortgat, M Mulders, I Neutelings, S Orfanelli, F Pantaleo, G Petrucciani, A Pfeiffer, M Pierini, H Qu, D Rabady, B Ribeiro Lopes, M Rovere, H Sakulin, S Sanchez Cruz, S Scarfi, C Schwick, M Selvaggi, A Sharma, K Shchelina, P Silva, P Sphicas[58], A G Stahl Leiton, A Steen, S Summers, D Treille, P Tropea, D Walter, J Wanczyk[59], J Wang, K A Wozniak[2], S Wuchterl, P Zehetner, P Zejdl, W D Zeuner
CERN, European Organization for Nuclear Research, Geneva, Switzerland

T Bevilacqua[60], L Caminada[60], A Ebrahimi, W Erdmann, R Horisberger, Q Ingram, H C Kaestli, D Kotlinski, C Lange, M Missiroli[60], L Noehte[60], T Rohe
Paul Scherrer Institut, Villigen, Switzerland

T K Aarrestad, K Androsov[59], M Backhaus, G Bonomelli, A Calandri, C Cazzaniga, K Datta, P De Bryas Dexmiers D'archiac[59], A De Cosa, G Dissertori, M Dittmar, M Donegà, F Eble, M Galli, K Gedia, F Glessgen, C Grab, N Härringer, T G Harte, D Hits, W Lustermann, A-M Lyon, R A Manzoni, M Marchegiani, L Marchese, C Martin Perez, A Mascellani[59], F Nessi-Tedaldi, F Pauss, V Perovic, S Pigazzini, C Reissel, B Ristic, F Riti, R Seidita, J Steggemann[59], A Tarabini, D Valsecchi, R Wallny
ETH Zurich - Institute for Particle Physics and Astrophysics (IPA), Zurich, Switzerland

C Amsler[61], P Bärtschi, M F Canelli, K Cormier, M Huwiler, W Jin, A Jofrehei, B Kilminster, S

Leontsinis, S P Liechti, A Macchiolo, P Meiring, F Meng, U Molinatti, J Motta, A Reimers, P Robmann, M Senger, E Shokr, F Stäger, R Tramontano
Universität Zürich, Zurich, Switzerland

C Adloff[62], D Bhowmik, C M Kuo, W Lin, P K Rout, P C Tiwari[37], S S Yu
National Central University, Chung-Li, Taiwan

L Ceard, K F Chen, P S Chen, Z G Chen, A De Iorio, W-S Hou, T H Hsu, Y W Kao, S Karmakar, G Kole, Y Y Li, R-S Lu, E Paganis, X F Su, J Thomas-Wilsker, L S Tsai, D Tsionou, H Y Wu, E Yazgan

National Taiwan University (NTU), Taipei, Taiwan

C Asawatangtrakuldee, N Srimanobhas, V Wachirapusitanand

High Energy Physics Research Unit, Department of Physics, Faculty of Science, Chulalongkorn University, Bangkok, Thailand

D Agyel, F Boran, F Dolek, I Dumanoglu[63], E Eskut, Y Guler[64], E Gurpinar Guler[64], C Isik, O Kara, A Kayis Topaksu, U Kiminsu, G Onengut, K Ozdemir[65], A Polatoz, B Tali[66], U G Tok, S Turkcapar, E Uslan, I S Zorbakir

Çukurova University, Physics Department, Science and Art Faculty, Adana, Turkey

G Sokmen, M Yalvac[67]
Middle East Technical University, Physics Department, Ankara, Turkey

B Akgun, I O Atakisi, E Gülmez, M Kaya[68], O Kaya[69], S Tekten[70]

Bogazici University, Istanbul, Turkey

A Cakir, K Cankocak[63,71], G G Dincer[63], Y Komurcu, S Sen[72]
Istanbul Technical University, Istanbul, Turkey

O Aydilek[73], B Hacisahinoglu, I Hos[74], B Kaynak, S Ozkorucuklu, O Potok, H Sert, C Simsek, C Zorbilmez
Istanbul University, Istanbul, Turkey

S Cerci[66], B Isildak[75], D Sunar Cerci, T Yetkin
Yildiz Technical University, Istanbul, Turkey

A Boyaryntsev, B Grynyov
Institute for Scintillation Materials of National Academy of Science of Ukraine, Kharkiv, Ukraine

L Levchuk
National Science Centre, Kharkiv Institute of Physics and Technology, Kharkiv, Ukraine

D Anthony, J J Brooke, A Bundock, F Bury, E Clement, D Cussans, H Flacher, M Glowacki, J Goldstein, H F Heath, M-L Holmberg, L Kreczko, S Paramesvaran, L Robertshaw, S Seif El Nasr-Storey, V J Smith, N Stylianou[76], K Walkingshaw Pass
University of Bristol, Bristol, United Kingdom

A H Ball, K W Bell, A Belyaev[77], C Brew, R M Brown, D J A Cockerill, C Cooke, A Elliot, K V Ellis, K Harder, S Harper, J Linacre, K Manolopoulos, D M Newbold, E Olaiya, D Petyt, T Reis, A R Sahasransu, G Salvi, T Schuh, C H Shepherd-Themistocleous, I R Tomalin, K C Whalen, T Williams
Rutherford Appleton Laboratory, Didcot, United Kingdom

I Andreou, R Bainbridge, P Bloch, C E Brown, O Buchmuller, V Cacchio, C A Carrillo Montoya, G S Chahal[78], D Colling, J S Dancu, I Das, P Dauncey, G Davies, J Davies, M Della Negra, S Fayer, G Fedi, G Hall, M H Hassanshahi, A Howard, G Iles, C R Knight, J Langford, J León Holgado, L Lyons, A-M Magnan, S Mallios, M Mieskolainen, J Nash[79], M Pesaresi, P B Pradeep, B C Radburn-Smith, A Richards, A Rose, K Savva, C Seez, R Shukla, A Tapper, K Uchida, G P Uttley, L H Vage, T Virdee[29], M Vojinovic, N Wardle, D Winterbottom
Imperial College, London, United Kingdom

K Coldham, J E Cole, A Khan, P Kyberd, I D Reid
Brunel University, Uxbridge, United Kingdom

S Abdullin, A Brinkerhoff, E Collins, M R Darwish[80], J Dittmann, K Hatakeyama, J Hiltbrand, B McMaster, J Samudio, S Sawant, C Sutantawibul, J Wilson
Baylor University, Waco, TX, United States of America

R Bartek, A Dominguez, C Huerta Escamilla, A E Simsek, R Uniyal, A M Vargas Hernandez
Catholic University of America, Washington, DC, United States of America

B Bam, A Buchot Perraguin, R Chudasama, S I Cooper, C Crovella, S V Gleyzer, E Pearson, C U Perez, P Rumerio[81], E Usai, R Yi
The University of Alabama, Tuscaloosa, AL, United States of America

A Akpinar, C Cosby, G De Castro, Z Demiragli, C Erice, C Fangmeier, C Fernandez Madrazo, E Fontanesi, D Gastler, F Golf, S Jeon, J O'cain, I Reed, J Rohlf, K Salyer, D Sperka, D Spitzbart, I Suarez, A Tsatsos, A G Zecchinelli

Boston University, Boston, MA, United States of America

G Benelli, D Cutts, L Gouskos, M Hadley, U Heintz, J M Hogan[82], T Kwon, G Landsberg, K T Lau, D Li, J Luo, S Mondal, N Pervan, T Russell, S Sagir[83], F Simpson, M Stamenkovic, N Venkatasubramanian, X Yan
Brown University, Providence, RI, United States of America

S Abbott, C Brainerd, R Breedon, H Cai, M Calderon De La Barca Sanchez, M Chertok, M Citron, J Conway, P T Cox, R Erbacher, F Jensen, O Kukral, G Mocellin, M Mulhearn, S Ostrom, W Wei, Y Yao, S Yoo, F Zhang
University of California, Davis, Davis, CA, United States of America

M Bachtis, R Cousins, A Datta, G Flores Avila, J Hauser, M Ignatenko, M A Iqbal, T Lam, E Manca, A Nunez Del Prado, D Saltzberg, V Valuev
University of California, Los Angeles, CA, United States of America

R Clare, J W Gary, M Gordon, G Hanson, W Si
University of California, Riverside, Riverside, CA, United States of America

A Aportela, A Arora, J G Branson, S Cittolin, S Cooperstein, D Diaz, J Duarte, L Giannini, Y Gu, J Guiang, R Kansal, V Krutelyov, R Lee, J Letts, M Masciovecchio, F Mokhtar, S Mukherjee, M Pieri, M Quinnan, B V Sathia Narayanan, V Sharma, M Tadel, E Vourliotis, F Würthwein, Y Xiang, A Yagil
University of California, San Diego, La Jolla, CA, United States of America

A Barzdukas, L Brennan, C Campagnari, K Downham, C Grieco, J Incandela, J Kim, A J Li, P Masterson, H Mei, J Richman, S N Santpur, U Sarica, R Schmitz, F Setti, J Sheplock, D Stuart, T Á. Vámi, S Wang, D Zhang
University of California, Santa Barbara - Department of Physics, Santa Barbara, CA, United States of America

S Bhattacharya, A Bornheim, O Cerri, A Latorre, J Mao, H B Newman, G Reales Gutiérrez, M Spiropulu, J R Vlimant, C Wang, S Xie, R Y Zhu
California Institute of Technology, Pasadena, CA, United States of America

J Alison, S An, P Bryant, M Cremonesi, V Dutta, T Ferguson, T A Gómez Espinosa, A Harilal, A Kallil Tharayil, C Liu, T Mudholkar, S Murthy, P Palit, K Park, M Paulini, A Roberts, A Sanchez, W Terrill
Carnegie Mellon University, Pittsburgh, PA, United States of America

J P Cumalat, W T Ford, A Hart, A Hassani, G Karathanasis, N Manganelli, J Pearkes, C Savard, N Schonbeck, K Stenson, K A Ulmer, S R Wagner, N Zipper, D Zuolo
University of Colorado Boulder, Boulder, CO, United States of America

J Alexander, S Bright-Thonney, X Chen, D J Cranshaw, J Fan, X Fan, S Hogan, P Kotamnives, J Monroy, M Oshiro, J R Patterson, M Reid, A Ryd, J Thom, P Wittich, R Zou
Cornell University, Ithaca, NY, United States of America

M Albrow, M Alyari, O Amram, G Apollinari, A Apresyan, L A T Bauerdick, D Berry, J Berryhill, P C Bhat, K Burkett, J N Butler, A Canepa, G B Cerati, H W K Cheung, F Chlebana, G Cummings, J Dickinson, I Dutta, V D Elvira, Y Feng, J Freeman, A Gandrakota, Z Gecse, L Gray, D Green, A Grummer, S Grünendahl, D Guerrero, O Gutsche, R M Harris, R Heller, T C Herwig, J Hirschauer, B Jayatilaka, S Jindariani, M Johnson, U Joshi, T Klijnsma, B Klima, K H M Kwok, S Lammel, D Lincoln, R Lipton, T Liu, C Madrid, K Maeshima, C Mantilla, D Mason, P McBride, P Merkel, S Mrenna, S Nahn, J Ngadiuba, D Noonan, S Norberg, V Papadimitriou, N Pastika, K Pedro, C Pena[84], F Ravera, A Reinsvold Hall[85], L Ristori, M Safdari, E Sexton-Kennedy, N Smith, A Soha, L Spiegel, S Stoynev, J Strait, L Taylor, S Tkaczyk, N V Tran, L Uplegger, E W Vaandering, I Zoi
Fermi National Accelerator Laboratory, Batavia, IL, United States of America

C Aruta, P Avery, D Bourilkov, P Chang, V Cherepanov, R D Field, E Koenig, M Kolosova, J Konigsberg, A Korytov, K Matchev, N Menendez, G Mitselmakher, K Mohrman, A Muthirakalayil Madhu, N Rawal, S Rosenzweig, Y Takahashi, J Wang
University of Florida, Gainesville, FL, United States of America

T Adams, A Al Kadhim, A Askew, S Bower, V Hagopian, R Hashmi, R S Kim, S Kim, T Kolberg, G Martinez, H Prosper, P R Prova, M Wulansatiti, R Yohay, J Zhang
Florida State University, Tallahassee, FL, United States of America

B Alsufyani, M M Baarmand, S Butalla, S Das, T Elkafrawy[86], M Hohlmann, E Yanes

Florida Institute of Technology, Melbourne, FL, United States of America

M R Adams, A Baty, C Bennett, R Cavanaugh, R Escobar Franco, O Evdokimov, C E Gerber, M Hawksworth, A Hingrajiya, D J Hofman, J H Lee, D S Lemos, A H Merrit, C Mills, S Nanda, G Oh, B Ozek, D Pilipovic, R Pradhan, E Prifti, T Roy, S Rudrabhatla, M B Tonjes, N Varelas, M A Wadud, Z Ye, J Yoo
University of Illinois Chicago, Chicago, United States of America

M Alhusseini, D Blend, K Dilsiz[87], L Emediato, G Karaman, O K Köseyan, J-P Merlo, A Mestvirishvili[88], O Neogi, H Ogul[89], Y Onel, A Penzo, C Snyder, E Tiras[90]

The University of Iowa, Iowa City, IA, United States of America

B Blumenfeld, L Corcodilos, J Davis, A V Gritsan, L Kang, S Kyriacou, P Maksimovic, M Roguljic, J Roskes, S Sekhar, M Swartz

Johns Hopkins University, Baltimore, MD, United States of America

A Abreu, L F Alcerro Alcerro, J Anguiano, S Arteaga Escatel, P Baringer, A Bean, Z Flowers, D Grove, J King, G Krintiras, M Lazarovits, C Le Mahieu, J Marquez, M Murray, M Nickel, M Pitt, S Popescu[91], C Rogan, C Royon, R Salvatico, S Sanders, C Smith, G Wilson
The University of Kansas, Lawrence, KS, United States of America

B Allmond, R Gujju Gurunadha, A Ivanov, K Kaadze, Y Maravin, J Natoli, D Roy, G Sorrentino
Kansas State University, Manhattan, KS, United States of America

A Baden, A Belloni, J Bistany-riebman, Y M Chen, S C Eno, N J Hadley, S Jabeen, R G Kellogg, T Koeth, B Kronheim, Y Lai, S Lascio, A C Mignerey, S Nabili, C Palmer, C Papageorgakis, M M Paranjpe, E Popova[92], A Shevelev, L Wang
University of Maryland, College Park, MD, United States of America

J Bendavid, I A Cali, P C Chou, M D'Alfonso, J Eysermans, C Freer, G Gomez-Ceballos, M Goncharov, G Grosso, P Harris, D Hoang, D Kovalskyi, J Krupa, L Lavezzo, Y-J Lee, K Long, C Mcginn, A Novak, C Paus, C Roland, G Roland, S Rothman, G S F Stephans, Z Wang, B Wyslouch, T J Yang
Massachusetts Institute of Technology, Cambridge, MA, United States of America

B Crossman, B M Joshi, C Kapsiak, M Krohn, D Mahon, J Mans, B Marzocchi, M Revering, R Rusack, R Saradhy, N Strobbe
University of Minnesota, Minneapolis, MN, United States of America

K Bloom, D R Claes, G Haza, J Hossain, C Joo, I Kravchenko, J E Siado, W Tabb, A Vagnerini, A Wightman, F Yan, D Yu
University of Nebraska-Lincoln, Lincoln, NE, United States of America

H Bandyopadhyay, L Hay, H w Hsia, I Iashvili, A Kalogeropoulos, A Kharchilava, M Morris, D Nguyen, J Pekkanen, S Rappoccio, H Rejeb Sfar, A Williams, P Young
State University of New York at Buffalo, Buffalo, NY, United States of America

G Alverson, E Barberis, J Bonilla, J Dervan, Y Haddad, Y Han, A Krishna, J Li, M Lu, G Madigan, R Mccarthy, D M Morse, V Nguyen, T Orimoto, A Parker, L Skinnari, D Wood
Northeastern University, Boston, MA, United States of America

J Bueghly, S Dittmer, K A Hahn, Y Liu, Y Miao, D G Monk, M H Schmitt, A Taliercio, M Velasco
Northwestern University, Evanston, IL, United States of America

G Agarwal, R Band, R Bucci, S Castells, A Das, R Goldouzian, M Hildreth, K W Ho, K Hurtado Anampa, T Ivanov, C Jessop, K Lannon, J Lawrence, N Loukas, L Lutton, J Mariano, N Marinelli, I Mcalister, T McCauley, C Mcgrady, C Moore, Y Musienko[17], H Nelson, M Osherson, A Piccinelli, R Ruchti, A Townsend, Y Wan, M Wayne, H Yockey, M Zarucki, L Zygala
University of Notre Dame, Notre Dame, IN, United States of America

A Basnet, B Bylsma, M Carrigan, L S Durkin, C Hill, M Joyce, M Nunez Ornelas, K Wei, B L Winer, B R Yates
The Ohio State University, Columbus, OH, United States of America

H Bouchamaoui, P Das, G Dezoort, P Elmer, A Frankenthal, B Greenberg, N Haubrich, K Kennedy, G Kopp, S Kwan, D Lange, A Loeliger, D Marlow, I Ojalvo, J Olsen, D Stickland, C Tully
Princeton University, Princeton, NJ, United States of America

S Malik
University of Puerto Rico, Mayaguez, PR, United States of America

A S Bakshi, S Chandra, R Chawla, A Gu, L Gutay, M Jones, A W Jung, A M Koshy, M Liu, G Negro, N Neumeister, G Paspalaki, S Piperov, V Scheurer, J F Schulte, M Stojanovic, J Thieman, A K Virdi, F Wang, A Wildridge, W Xie

Purdue University, West Lafayette, IN, United States of America

J Dolen, N Parashar, A Pathak

Purdue University Northwest, Hammond, IN, United States of America

D Acosta, T Carnahan, K M Ecklund, P J Fernández Manteca, S Freed, P Gardner, F J M Geurts, I Krommydas, W Li, J Lin, O Miguel Colin, B P Padley, R Redjimi, J Rotter, E Yigitbasi, Y Zhang

Rice University, Houston, TX, United States of America

A Bodek, P de Barbaro, R Demina, J L Dulemba, A Garcia-Bellido, O Hindrichs, A Khukhunaishvili, N Parmar, P Parygin[92], R Taus

University of Rochester, Rochester, NY, United States of America

B Chiarito, J P Chou, S V Clark, D Gadkari, Y Gershtein, E Halkiadakis, M Heindl, C Houghton, D Jaroslawski, S Konstantinou, I Laflotte, A Lath, R Montalvo, K Nash, J Reichert, H Routray, P Saha, S Salur, S Schnetzer, S Somalwar, R Stone, S A Thayil, S Thomas, J Vora, H Wang

Rutgers, The State University of New Jersey, Piscataway, NJ, United States of America

D Ally, A G Delannoy, S Fiorendi, S Higginbotham, T Holmes, A R Kanuganti, N Karunarathna, L Lee, E Nibigira, S Spanier

University of Tennessee, Knoxville, TN, United States of America

D Aebi, M Ahmad, T Akhter, O Bouhali[93], R Eusebi, J Gilmore, T Huang, T Kamon[94], H Kim, S Luo, R Mueller, D Overton, D Rathjens, A Safonov

Texas A&M University, College Station, TX, United States of America

N Akchurin, J Damgov, N Gogate, V Hegde, A Hussain, Y Kazhykarim, K Lamichhane, S W Lee, A Mankel, T Peltola, I Volobouev

Texas Tech University, Lubbock, TX, United States of America

E Appelt, Y Chen, S Greene, A Gurrola, W Johns, R Kunnawalkam Elayavalli, A Melo, F Romeo, P Sheldon, S Tuo, J Velkovska, J Viinikainen

Vanderbilt University, Nashville, TN, United States of America

B Cardwell, H Chung, B Cox, J Hakala, R Hirosky, A Ledovskoy, C Neu

University of Virginia, Charlottesville, VA, United States of America

S Bhattacharya, P E Karchin

Wayne State University, Detroit, MI, United States of America

A Aravind, S Banerjee, K Black, T Bose, S Dasu, I De Bruyn, P Everaerts, C Galloni, H He, M Herndon, A Herve, C K Koraka, A Lanaro, R Loveless, J Madhusudanan Sreekala, A Mallampalli, A Mohammadi, S Mondal, G Parida, L Pétré, D Pinna, A Savin, V Shang, V Sharma, W H Smith, D Teague, H F Tsoi, W Vetens, A Warden

University of Wisconsin - Madison, Madison, WI, United States of America

S Afanasiev, V Alexakhin, V Andreev, Yu Andreev, T Aushev, M Azarkin, A Babaev, V Blinov[95], E Boos, V Borshch, D Budkouski, V Bunichev, V Chekhovsky, R Chistov[95], M Danilov[95], A Dermenev, T Dimova[95], D Druzhkin[96], M Dubinin[84], L Dudko, A Ershov, G Gavrilov, V Gavrilov, S Gninenko, V Golovtcov, N Golubev, I Golutvin†, I Gorbunov, Y Ivanov, V Kachanov, V Karjavine, A Karneyeu, V Kim[95], M Kirakosyan, D Kirpichnikov, M Kirsanov, V Klyukhin, D Konstantinov, V Korenkov, A Kozyrev[95], N Krasnikov, A Lanev, P Levchenko[97], N Lychkovskaya, V Makarenko, A Malakhov, A Markina, V Matveev[95], V Murzin, A Nikitenko[98,99], S Obraztsov, V Oreshkin, V Palichik, V Perelygin, M Perfilov, S Polikarpov[95], V Popov, O Radchenko[95], M Savina, V Savrin, V Shalaev, S Shmatov, S Shulha, Y Skovpen[95], S Slabospitskii, V Smirnov, D Sosnov, V Sulimov, A Terkulov, O Teryaev, I Tlisova, A Toropin, L Uvarov, A Uzunian, P Volkov, A Vorobyev†, G Vorotnikov, N Voytishin, B S Yuldashev[100], A Zarubin, I Zhizhin, A Zhokin

Authors affiliated with an institute or an international laboratory covered by a cooperation agreement with CERN

†Deceased
[1]Also at Yerevan State University, Yerevan, Armenia
[2]Also at University of Vienna, Vienna, Austria
[3]Also at TU Wien, Vienna, Austria
[4]Also at Ghent University, Ghent, Belgium

[5]Also at Universidade do Estado do Rio de Janeiro, Rio de Janeiro, Brazil
[6]Also at Universidade Estadual de Campinas, Campinas, Brazil
[7]Also at Federal University of Rio Grande do Sul, Porto Alegre, Brazil
[8]Also at UFMS, Nova Andradina, Brazil
[9]Also at Nanjing Normal University, Nanjing, People's Republic of China
[10]Now at The University of Iowa, Iowa City, IA, United States of America
[11]Also at University of Chinese Academy of Sciences, Beijing, People's Republic of China
[12]Also at China Center of Advanced Science and Technology, Beijing, People's Republic of China
[13]Also at University of Chinese Academy of Sciences, Beijing, People's Republic of China
[14]Also at China Spallation Neutron Source, Guangdong, People's Republic of China
[15]Now at Henan Normal University, Xinxiang, People's Republic of China
[16]Also at Université Libre de Bruxelles, Bruxelles, Belgium
[17]Also at an institute or an international laboratory covered by a cooperation agreement with CERN
[18]Also at Suez University, Suez, Egypt
[19]Now at British University in Egypt, Cairo, Egypt
[20]Also at Purdue University, West Lafayette, IN, United States of America
[21]Also at Université de Haute Alsace, Mulhouse, France
[22]Also at Istinye University, Istanbul, Turkey
[23]Also at The University of the State of Amazonas, Manaus, Brazil
[24]Also at University of Hamburg, Hamburg, Germany
[25]Also at RWTH Aachen University, III. Physikalisches Institut A, Aachen, Germany
[26]Also at Bergische University Wuppertal (BUW), Wuppertal, Germany
[27]Also at Brandenburg University of Technology, Cottbus, Germany
[28]Also at Forschungszentrum Jülich, Juelich, Germany
[29]Also at CERN, European Organization for Nuclear Research, Geneva, Switzerland
[30]Also at Institute of Nuclear Research ATOMKI, Debrecen, Hungary
[31]Now at Universitatea Babes-Bolyai - Facultatea de Fizica, Cluj-Napoca, Romania
[32]Also at MTA-ELTE Lendület CMS Particle and Nuclear Physics Group, Eötvös Loránd University, Budapest, Hungary
[33]Also at HUN-REN Wigner Research Centre for Physics, Budapest, Hungary
[34]Also at Physics Department, Faculty of Science, Assiut University, Assiut, Egypt
[35]Also at Punjab Agricultural University, Ludhiana, India
[36]Also at University of Visva-Bharati, Santiniketan, India
[37]Also at Indian Institute of Science (IISc), Bangalore, India
[38]Also at IIT Bhubaneswar, Bhubaneswar, India
[39]Also at Institute of Physics, Bhubaneswar, India
[40]Also at University of Hyderabad, Hyderabad, India
[41]Also at Deutsches Elektronen-Synchrotron, Hamburg, Germany
[42]Also at Isfahan University of Technology, Isfahan, Iran
[43]Also at Sharif University of Technology, Tehran, Iran
[44]Also at Department of Physics, University of Science and Technology of Mazandaran, Behshahr, Iran
[45]Also at Department of Physics, Isfahan University of Technology, Isfahan, Iran
[46]Also at Department of Physics, Faculty of Science, Arak University, Arak, Iran
[47]Also at Helwan University, Cairo, Egypt
[48]Also at Italian National Agency for New Technologies, Energy and Sustainable Economic Development, Bologna, Italy
[49]Also at Centro Siciliano di Fisica Nucleare e di Struttura Della Materia, Catania, Italy
[50]Also at Università degli Studi Guglielmo Marconi, Roma, Italy
[51]Also at Scuola Superiore Meridionale, Università di Napoli 'Federico II', Napoli, Italy
[52]Also at Fermi National Accelerator Laboratory, Batavia, IL, United States of America
[53]Also at Consiglio Nazionale delle Ricerche - Istituto Officina dei Materiali, Perugia, Italy
[54]Also at Department of Applied Physics, Faculty of Science and Technology, Universiti Kebangsaan Malaysia, Bangi, Malaysia
[55]Also at Consejo Nacional de Ciencia y Tecnología, Mexico City, Mexico
[56]Also at Trincomalee Campus, Eastern University, Sri Lanka, Nilaveli, Sri Lanka
[57]Also at Saegis Campus, Nugegoda, Sri Lanka
[58]Also at National and Kapodistrian University of Athens, Athens, Greece
[59]Also at Ecole Polytechnique Fédérale Lausanne, Lausanne, Switzerland
[60]Also at Universität Zürich, Zurich, Switzerland
[61]Also at Stefan Meyer Institute for Subatomic Physics, Vienna, Austria
[62]Also at Laboratoire d'Annecy-le-Vieux de Physique des Particules, IN2P3-CNRS, Annecy-le-Vieux, France
[63]Also at Near East University, Research Center of Experimental Health Science, Mersin, Turkey
[64]Also at Konya Technical University, Konya, Turkey
[65]Also at Izmir Bakircay University, Izmir, Turkey
[66]Also at Adiyaman University, Adiyaman, Turkey
[67]Also at Bozok Universitetesi Rektörlügü, Yozgat, Turkey
[68]Also at Marmara University, Istanbul, Turkey
[69]Also at Milli Savunma University, Istanbul, Turkey
[70]Also at Kafkas University, Kars, Turkey
[71]Now at Istanbul Okan University, Istanbul, Turkey
[72]Also at Hacettepe University, Ankara, Turkey
[73]Also at Erzincan Binali Yildirim University, Erzincan, Turkey
[74]Also at Istanbul University - Cerrahpasa, Faculty of Engineering, Istanbul, Turkey
[75]Also at Yildiz Technical University, Istanbul, Turkey
[76]Also at Vrije Universiteit Brussel, Brussel, Belgium

[77]Also at School of Physics and Astronomy, University of Southampton, Southampton, United Kingdom
[78]Also at IPPP Durham University, Durham, United Kingdom
[79]Also at Monash University, Faculty of Science, Clayton, Australia
[80]Also at Institute of Basic and Applied Sciences, Faculty of Engineering, Arab Academy for Science, Technology and Maritime Transport, Alexandria, Egypt
[81]Also at Università di Torino, Torino, Italy
[82]Also at Bethel University, St. Paul, MN, United States of America
[83]Also at Karamanoğlu Mehmetbey University, Karaman, Turkey
[84]Also at California Institute of Technology, Pasadena, CA, United States of America
[85]Also at United States Naval Academy, Annapolis, MD, United States of America
[86]Also at Ain Shams University, Cairo, Egypt
[87]Also at Bingol University, Bingol, Turkey
[88]Also at Georgian Technical University, Tbilisi, Georgia
[89]Also at Sinop University, Sinop, Turkey
[90]Also at Erciyes University, Kayseri, Turkey
[91]Also at Horia Hulubei National Institute of Physics and Nuclear Engineering (IFIN-HH), Bucharest, Romania
[92]Now at an institute or an international laboratory covered by a cooperation agreement with CERN
[93]Also at Texas A&M University at Qatar, Doha, Qatar
[94]Also at Kyungpook National University, Daegu, Republic of Korea
[95]Also at another institute or international laboratory covered by a cooperation agreement with CERN
[96]Also at Universiteit Antwerpen, Antwerpen, Belgium
[97]Also at Northeastern University, Boston, MA, United States of America
[98]Also at Imperial College, London, United Kingdom
[99]Now at Yerevan Physics Institute, Yerevan, Armenia
[100]Also at Institute of Nuclear Physics of the Uzbekistan Academy of Sciences, Tashkent, Uzbekistan

References

[1] Freedman S J and Clauser J F 1972 Experimental test of local hidden-variable theories *Phys. Rev. Lett.* **28** 938
[2] Aspect A, Dalibard J and Roger G 1982 Experimental test of Bell's inequalities using time-varying analyzers *Phys. Rev. Lett.* **49** 1804
[3] Vaziri A, Weihs G and Zeilinger A 2002 Experimental two-photon, three-dimensional entanglement for quantum communication *Phys. Rev. Lett.* **89** 240401
[4] Aspect A, Grangier P and Roger G 1982 Experimental realization of Einstein–Podolsky–Rosen–Bohm *gedankenexperiment*: a new violation of Bell's inequalities *Phys. Rev. Lett.* **49** 91
[5] Hensen B *et al* 2015 Loophole-free Bell inequality violation using electron spins separated by 1.3 kilometres *Nature* **526** 682
[6] Giustina M *et al* 2015 Significant-loophole-free test of Bell's theorem with entangled photons *Phys. Rev. Lett.* **115** 250401
[7] Pfaff W *et al* 2012 Demonstration of entanglement-by-measurement of solid-state qubits *Nat. Phys.* **9** 29
[8] Bell J S 1964 On the Einstein–Podolsky–Rosen paradox *Phys. Phys. Fiz.* **1** 195
[9] Rowe M A, Kielpinski D, Meyer V, Sackett C A, Itano W M, Monroe C and Wineland D J 2001 Experimental violation of a Bell's inequality with efficient detection *Nature* **409** 791
[10] Ansmann M *et al* 2009 Violation of Bell's inequality in Josephson phase qubits *Nature* **461** 504
[11] Einstein A, Podolsky B and Rosen N 1935 Can quantum-mechanical description of physical reality be considered complete? *Phys. Rev.* **47** 777
[12] Barr A J, Caban P and Rembieliński J 2023 Bell-type inequalities for systems of relativistic vector bosons *Quantum* **7** 1070
[13] Barr A J 2022 Testing Bell inequalities in Higgs boson decays *Phys. Lett.* B **825** 136866
[14] Aguilar-Saavedra J A 2023 Laboratory-frame tests of quantum entanglement in $H \to WW$ *Phys. Rev.* D **107** 076016
[15] Aguilar-Saavedra J A, Bernal A, Casas J A and Moreno J M 2023 Testing entanglement and Bell inequalities in $H \to ZZ$ *Phys. Rev.* D **107** 016012
[16] Altakach M M *et al* 2023 Quantum information and *CP* measurement in $H \to \tau^+\tau^-$ at future lepton colliders *Phys. Rev.* D **107** 093002
[17] Cheng K, Han T and Low M 2024 Optimizing fictitious states for Bell inequality violation in bipartite qubit systems with applications to the $t\bar{t}$ system *Phys. Rev.* D **109** 116005
[18] Han T, Low M and Wu T A 2024 Quantum entanglement and Bell inequality violation in semi-leptonic top decays *J. High Energy Phys.* JHEP07(2024)192
[19] Dong Z, Gonçalves D, Kong K and Navarro A 2024 Entanglement and Bell inequalities with boosted $t\bar{t}$ *Phys. Rev.* D **109** 115023
[20] Varma M and Baker O K 2024 Quantum entanglement in top quark pair production *Nucl. Phys.* A **1042** 122795
[21] Barr A J, Fabbrichesi M, Floreanini R, Gabrielli E and Marzola L 2024 Quantum entanglement and Bell inequality violation at colliders *Prog. Part. Nucl. Phys.* **139** 104134
[22] Fabbrichesi M, Floreanini R, Gabrielli E and Marzola L 2023 Bell inequalities and quantum entanglement in weak gauge boson production at the LHC and future colliders *Eur. Phys. J.* C **83** 823
[23] Cheng K, Han T and Low M 2024 Optimizing entanglement and Bell inequality violation in top anti-top events (arXiv:2407.01672)
[24] Abel S A, Dittmar M and Dreiner H 1992 Testing locality at colliders via Bell's inequality? *Phys. Lett.* B **280** 304
[25] Fabbrichesi M, Floreanini R, Gabrielli E and Marzola L 2024 Bell inequality is violated in $B^0 \to J/\psi K^*(892)^0$ decays *Phys. Rev.* D **109** L031104
[26] ATLAS Collaboration 2023 Observation of quantum entanglement in top-quark pairs using the ATLAS detector *Nature* **633** 542
[27] Afik Y and de Nova J R M 2021 Entanglement and quantum tomography with top quarks at the LHC *Eur. Phys. J. Plus* **136** 907

[28] Fabbrichesi M, Floreanini R and Panizzo G 2021 Testing Bell inequalities at the LHC with top-quark pairs *Phys. Rev. Lett.* **127** 161801

[29] Severi C, Degli Esposti Boschi C, Maltoni F and Sioli M 2022 Quantum tops at the LHC: from entanglement to Bell inequalities *Eur. Phys. J.* C **82** 285

[30] Iengo R 2009 Sommerfeld enhancement: general results from field theory diagrams *J. High Energy Phys.* JHEP05(2009)024

[31] Mammen Abraham R and Gonçalves D 2023 Boosting new physics searches in $t\bar{t}Z$ and tZj production with angular moments *Eur. Phys. J.* C **83** 965

[32] Gonçalves D, Kim J H, Kong K and Wu Y 2022 Direct Higgs-top *CP*-phase measurement with $t\bar{t}h$ at the 14 TeV LHC and 100 TeV FCC *J. High Energy Phys.* JHEP01(2022)158

[33] Aoude R, Madge E, Maltoni F and Mantani L 2022 Quantum SMEFT tomography: top quark pair production at the LHC *Phys. Rev.* D **106** 055007

[34] Baer H, Barger V, Dutta J, Sengupta D and Zhang K 2023 Top squarks from the landscape at high luminosity LHC *Phys. Rev.* D **108** 075027

[35] Severi C and Vryonidou E 2023 Quantum entanglement and top spin correlations in SMEFT at higher orders *J. High Energy Phys.* JHEP01(2023)148

[36] Fabbrichesi M, Floreanini R and Gabrielli E 2023 Constraining new physics in entangled two-qubit systems: top-quark, tau-lepton and photon pairs *Eur. Phys. J.* C **83** 162

[37] Maltoni F, Severi C, Tentori S and Vryonidou E 2024 Quantum detection of new physics in top-quark pair production at the LHC *J. High Energy Phys.* JHEP03(2024)099

[38] Maltoni F, Severi C, Tentori S and Vryonidou E 2024 Quantum tops at circular lepton colliders (arXiv:2404.08049)

[39] Workman R L *et al* (Particle Data Group) 2022 Review of particle physics *Prog. Theor. Exp. Phys.* **2022** 083C01

[40] Mahlon G and Parke S J 2010 Spin correlation effects in top quark pair production at the LHC *Phys. Rev.* D **81** 074024

[41] CMS Collaboration 2019 Measurement of the top quark polarization and $t\bar{t}$ spin correlations using dilepton final states in proton-proton collisions at $\sqrt{s} = 13$ TeV *Phys. Rev.* D **100** 072002

[42] Czakon M and Mitov A 2014 Top++: a program for the calculation of the top-pair cross-section at hadron colliders *Comput. Phys. Commun.* **185** 2930

[43] Czakon M and Mitov A 2012 NNLO corrections to top-pair production at hadron colliders: the all-fermionic scattering channels *J. High Energy Phys.* JHEP12(2012)054

[44] Czakon M and Mitov A 2013 NNLO corrections to top pair production at hadron colliders: the quark-gluon reaction *J. High Energy Phys.* JHEP01(2013)080

[45] Czakon M, Fiedler P and Mitov A 2013 Total top-quark pair-production cross section at hadron colliders through $\mathcal{O}(\alpha_S^4)$ *Phys. Rev. Lett.* **110** 252004

[46] Fuks B, Hagiwara K, Ma K and Zheng Y-J 2021 Signatures of toponium formation in LHC run 2 data *Phys. Rev.* D **104** 034023

[47] Brambilla N, Pineda A, Soto J and Vairo A 2000 Potential NRQCD: an effective theory for heavy quarkonium *Nucl. Phys.* B **566** 275

[48] CMS Collaboration 2024 Differential cross section measurements for the production of top quark pairs and of additional jets using dilepton events from pp collisions at $\sqrt{s} = 13$ TeV *J. High Energy Phys.* (submitted) (arXiv:2402.08486)

[49] CMS Collaboration 2019 Measurements of $t\bar{t}$ differential cross sections in proton-proton collisions at $\sqrt{s} = 13$ TeV using events containing two leptons *J. High Energy Phys.* JHEP02(2019)149

[50] CMS Collaboration 2017 Measurement of differential cross sections for top quark pair production using the lepton+jets final state in proton-proton collisions at 13 TeV *Phys. Rev.* D **95** 092001

[51] ATLAS Collaboration 2018 Measurements of $t\bar{t}$ differential cross-sections of highly boosted top quarks decaying to all-hadronic final states in pp collisions at $\sqrt{s} = 13$ TeV using the ATLAS detector *Phys. Rev.* D **98** 012003

[52] ATLAS Collaboration 2020 Measurement of the $t\bar{t}$ production cross-section in the lepton+jets channel at $\sqrt{s} = 13$ TeV with the ATLAS experiment *Phys. Lett.* B **810** 135797

[53] Kiyo Y, Kühn J H, Moch S, Steinhauser M and Uwer P 2009 Top-quark pair production near threshold at LHC *Eur. Phys. J.* C **60** 375

[54] Ju W-L, Wang G, Wang X, Xu X, Xu Y and Yang L L 2020 Top quark pair production near threshold: single/double distributions and mass determination *J. High Energy Phys.* JHEP06(2020)158

[55] Sumino Y and Yokoya H 2010 Bound-state effects on kinematical distributions of top quarks at hadron colliders *J. High Energy Phys.* JHEP09(2010)034
Sumino Y and Yokoya H 2016 *J. High Energy Phys.* JHEP06(2016)037 (erratum)

[56] Fadin V S, Khoze V A and Sjöstrand T 1990 On the threshold behaviour of heavy top production *Z. Phys.* C **48** 613

[57] Beneke M, Garny M, Jaskiewicz S, Strohm J, Szafron R, Vernazza L and Wang J 2022 Next-to-leading power endpoint factorization and resummation for off-diagonal 'gluon' thrust *J. High Energy Phys.* JHEP07(2022)144

[58] Mahlon G and Parke S J 1996 Angular correlations in top quark pair production and decay at hadron colliders *Phys. Rev.* D **53** 4886

[59] Bernreuther W, Heisler D and Si Z-G 2015 A set of top quark spin correlation and polarization observables for the LHC: standard model predictions and new physics contributions *J. High Energy Phys.* JHEP12(2015)026

[60] Brandenburg A, Si Z G and Uwer P 2002 QCD-corrected spin analysing power of jets in decays of polarized top quarks *Phys. Lett.* B **539** 235

[61] CDF Collaboration 2011 Measurement of $t\bar{t}$ spin correlation in $p\bar{p}$ collisions using the CDF II detector at the Tevatron *Phys. Rev.* D **83** 031104

[62] Peres A 1996 Separability criterion for density matrices *Phys. Rev. Lett.* **77** 1413

[63] Horodecki M, Horodecki P and Horodecki R 1996 On the necessary and sufficient conditions for separability of mixed quantum states *Phys. Lett.* A **223** 1

[64] Baumgart M and Tweedie B 2013 A new twist on top quark spin correlations *J. High Energy Phys.* JHEP03(2013)117

[65] Horodecki R, Horodecki P and Horodecki M 1995 Violating Bell inequality by mixed spin-1/2 states: necessary and sufficient condition *Phys. Lett.* A **200** 340

[66] Aguilar-Saavedra J A and Casas J A 2022 Improved tests of entanglement and Bell inequalities with LHC tops *Eur. Phys. J.* C **82** 666

[67] CMS Collaboration 2022 Projection of the top quark spin correlation measurement and search for top squark pair production at the HL-LHC *CMS Physics Analysis Summary* CMS-PAS-FTR-18-034 (available at: https://cds.cern.ch/record/2813262)

[68] CMS Collaboration 2024 The CMS statistical analysis and combination tool: COMBINE *Comput. Softw. Big Sci.* accepted (https://doi.org/10.1007/s41781-024-00121-4)

[69] Verkerke W and Kirkby D 2003 The RooFit toolkit for data modeling *Proc. 13th Int. Conf. on Computing in High Energy and Nuclear Physics (CHEP 2003) (La Jolla CA, United States, 24–28 March 2003)* (eConf C0303241 (2003) MOLT007) (arXiv:physics/0306116) (available at: www.slac.stanford.edu/econf/C0303241/proc/papers/MOLT007.PDF)

[70] Moneta L *et al* 2010 The RooStats project *Proc. Sci.* **093** 057

[71] CMS Collaboration 2017 The CMS trigger system *JINST* **12** P01020

[72] CMS Collaboration 2008 The CMS experiment at the CERN LHC *JINST* **3** S08004

[73] CMS Collaboration 2024 Development of the CMS detector for the CERN LHC Run 3 *JINST* **19** P05064

[74] CMS Collaboration 2017 Particle-flow reconstruction and global event description with the CMS detector *JINST* **12** P10003

[75] Cacciari M, Salam G P and Soyez G 2008 The anti-k_T jet clustering algorithm *J. High Energy Phys.* JHEP04(2008)063

[76] Cacciari M, Salam G P and Soyez G 2012 FastJet user manual *Eur. Phys. J.* C **72** 1896

[77] CMS Collaboration 2020 Pileup mitigation at CMS in 13 TeV data *JINST* **15** P09018

[78] CMS Collaboration 2017 Jet energy scale and resolution in the CMS experiment in pp collisions at 8 TeV *JINST* **12** P02014

[79] CMS Collaboration 2019 Performance of missing transverse momentum reconstruction in proton-proton collisions at $\sqrt{s} = 13$ TeV using the CMS detector *JINST* **14** P07004

[80] CMS Collaboration 2015 Performance of electron reconstruction and selection with the CMS detector in proton-proton collisions at $\sqrt{s} = 8$ TeV *JINST* **10** P06005

[81] CMS Collaboration 2021 Electron and photon reconstruction and identification with the CMS experiment at the CERN LHC *JINST* **16** P05014

[82] CMS Collaboration 2020 ECAL 2016 refined calibration and Run 2 summary plots *CMS Detector Performance Note* CMS-DP-2020-021 (available at: https://cds.cern.ch/record/2717925)

[83] CMS Collaboration 2018 Performance of the CMS muon detector and muon reconstruction with proton-proton collisions at $\sqrt{s} = 13$ TeV *JINST* **13** P06015

[84] Frixione S, Ridolfi G and Nason P 2007 A positive-weight next-to-leading-order Monte Carlo for heavy flavour hadroproduction *J. High Energy Phys.* JHEP09(2007)126

[85] Nason P 2004 A new method for combining NLO QCD with shower Monte Carlo algorithms *J. High Energy Phys.* JHEP11(2004)040

[86] Frixione S, Nason P and Oleari C 2007 Matching NLO QCD computations with parton shower simulations: the POWHEG method *J. High Energy Phys.* JHEP11(2007)070

[87] Alioli S, Nason P, Oleari C and Re E 2010 A general framework for implementing NLO calculations in shower Monte Carlo programs: the POWHEG BOX *J. High Energy Phys.* JHEP06(2010)043

[88] Alwall J *et al* 2014 The automated computation of tree-level and next-to-leading order differential cross sections and their matching to parton shower simulations *J. High Energy Phys.* JHEP07(2014)079

[89] Artoisenet P, Frederix R, Mattelaer O and Rietkerk R 2013 Automatic spin-entangled decays of heavy resonances in Monte Carlo simulations *J. High Energy Phys.* JHEP03(2013)015

[90] Frederix R and Frixione S 2012 Merging meets matching in MC@NLO *J. High Energy Phys.* JHEP12(2012)061

[91] NNPDF Collaboration 2015 Parton distributions for the LHC run II *J. High Energy Phys.* JHEP04(2015)040

[92] Czakon M, Heymes D and Mitov A 2017 fastNLO tables for NNLO top-quark pair differential distributions (arXiv:1704.08551)

[93] Czakon M, Heymes D and Mitov A 2016 High-precision differential predictions for top-quark pairs at the LHC *Phys. Rev. Lett.* **116** 082003

[94] Czakon M, Heymes D and Mitov A 2017 Dynamical scales for multi-TeV top-pair production at the LHC *J. High Energy Phys.* JHEP04(2017)071

[95] CMS Collaboration 2020 Measurement of the top quark Yukawa coupling from $\mathrm{t\bar{t}}$ kinematic distributions in the dilepton final state in proton-proton collisions at $\sqrt{s} = 13$ TeV *Phys. Rev.* D **102** 092013

[96] Sjöstrand T *et al* 2015 An introduction to PYTHIA 8.2 *Comput. Phys. Commun.* **191** 159

[97] CMS Collaboration 2016 Investigations of the impact of the parton shower tuning in PYTHIA8 in the modelling of $\mathrm{t\bar{t}}$ at $\sqrt{s} = 8$ and 13 TeV *CMS Physics Analysis Summary* CMS-PAS-TOP-16-021 (available at: https://cds.cern.ch/record/2235192)

[98] CMS Collaboration 2016 Event generator tunes obtained from underlying event and multiparton scattering measurements *Eur. Phys. J.* C **76** 155

[99] Bähr M *et al* 2008 HERWIG++ physics and manual *Eur. Phys. J.* C **58** 639

[100] Gieseke S, Röhr C and Siodmok A 2012 Colour reconnections in HERWIG++ *Eur. Phys. J.* C **72** 2225

[101] GEANT4 Collaboration 2003 GEANT4—a simulation toolkit *Nucl. Instrum. Methods Phys. Res.* A **506** 250

[102] CMS Collaboration 2018 Identification of heavy-flavour jets with the CMS detector in pp collisions at 13 TeV *JINST* **13** P05011

[103] CMS Collaboration 2012 Measurement of the $\mathrm{t\bar{t}}$ production cross section in the dilepton channel in pp collisions at $\sqrt{s} = 7$ TeV *J. High Energy Phys.* JHEP11(2012)067

[104] CMS Collaboration 2015 Measurement of the differential cross section for top quark pair production in pp collisions at $\sqrt{s} = 8$ TeV *Eur. Phys. J.* C **75** 542

[105] CMS Collaboration 2016 Measurement of the top quark pair production cross section in proton-proton collisions at $\sqrt{s} = 13$ TeV *Phys. Rev. Lett.* **116** 052002

[106] CMS Collaboration 2011 Measurement of the Drell–Yan cross section in pp collisions at $\sqrt{s} = 7$ TeV *J. High Energy Phys.* JHEP10(2011)007

[107] CMS Collaboration 2018 Measurement of the inelastic proton-proton cross section at $\sqrt{s} = 13$ TeV *J. High Energy Phys.* JHEP07(2018)161

[108] CMS Collaboration 2021 Precision luminosity measurement in proton-proton collisions at $\sqrt{s} = 13$ TeV in 2015 and 2016 at CMS *Eur. Phys. J.* C **81** 800

[109] CMS Collaboration 2020 Extraction and validation of a new set of CMS PYTHIA 8 tunes from underlying-event measurements *Eur. Phys. J.* C **80** 4

[110] Christiansen J R and Skands P Z 2015 String formation beyond leading colour *J. High Energy Phys.* JHEP08(2015)003

[111] Argyropoulos S and Sjöstrand T 2014 Effects of color reconnection on $\mathrm{t\bar{t}}$ final states at the LHC *J. High Energy Phys.* JHEP11(2014)043

[112] Bowler M G 1981 e^+e^- production of heavy quarks in the string model *Z. Phys.* C **11** 169

[113] Andersson B, Gustafson G, Ingelman G and Sjöstrand T 1983 Parton fragmentation and string dynamics *Phys. Rep.* **97** 31

[114] CMS Collaboration 2021 Measurement of the shape of the b quark fragmentation function using charmed mesons produced inside b jets from $t\bar{t}$ pair decays *CMS Physics Analysis Summary* CMS-PAS-TOP-18-012 (available at: https://cds.cern.ch/record/2771694)

[115] CMS Collaboration 2024 Review of top quark mass measurements in CMS *Phys. Rep.* (submitted) (arXiv:2403.01313)

[116] Martin A 1988 Toponium physics *Quarks, Leptons and Their Constituents* ed A Zichichi (Springer) p 447

[117] 2024 HEPData record for this analysis (https://doi.org/10.17182/hepdata.145665)